Received June 16, 2021, accepted July 2, 2021, date of publication August 9, 2021, date of current version August 27, 2021.

Digital Object Identifier 10.1109/ACCESS.2021.3103848

Feature Extraction Methods for Electroretinogram Signal Analysis: A Review

SOROOR BEHBAHANI[1], HAMID AHMADIEH[2], AND SREERAMAN RAJAN[3], (Senior Member, IEEE)

[1]Department of Biomedical Engineering, Islamic Azad University, South Tehran Branch, Tehran 1777613651, Iran
[2]Ophthalmic Research Center, Research Institute for Ophthalmology and Vision Science, Shahid Beheshti University of Medical Sciences, Tehran 19857-17443, Iran
[3]Department of Systems and Computer Engineering, Carleton University, Ottawa, ON K1S 5B6, Canada

Corresponding author: Soroor Behbahani (sor.behbahani@gmail.com)

ABSTRACT Feature extraction is an essential aspect of electroretinogram (ERG) signal analysis. The extracted features are beneficial to analyze the signal further and compress the signal for storage or transmission purposes. Various methods have been widely employed to extract the characteristics of ERG signals. Methods based on the time-domain, frequency-domain, time-frequency domain and nonlinear and chaotic feature extraction techniques have been used to extract features that characterize ERG signals. This paper reviews several feature extraction methods applied to ERG and compares their performance under different conditions to provide guidance to select the most appropriate feature extraction method based on the performance.

INDEX TERMS Electroretinogram, feature extraction, frequency-domain analysis, time-domain analysis, time-frequency domain analysis, nonlinear analysis, retina.

I. INTRODUCTION

Electroretinogram (ERG) is the electrical response of different retinal cells to light and darkness. These cells include rod and cone photoreceptors, internal retinal cells (bipolar cells and amacrine), ganglion cells, and Müller cells [1]–[4]. The ERG is a short-duration signal that contains information about the complex nature of the retinal cell function.

Depending on retinal examination, there are different types of ERG recordings with various unstructured light stimuli (flashes). Full-field electroretinography (ffERG) is the conventional form of ERG that provides the summed electrical response of the entire retina evoked by a flashlight from Ganzfeld stimulus bow scattered in the eye through a dilated pupil [5]. Multifocal ERG (mfERG) is the best electrofunctional method used to study the retina's focal function in a quick and reproducible way [6], [7]. This is mainly used to diagnose and monitor macular disorders [8]. A specialized version of the ERG is the pattern ERG (PERG), which is used to study the function of the innermost retinal layers (early losses of retinal ganglion cells (RGCs) and fibers). PERG has shown a correlation with optic nerve integrity and can provide information from RGCs, which cannot be supplied by ffERG [9]. Besides these different types of ERG recordings, visual evoked potentials (VEP) also allow the assessment of the visual pathways through the optic nerve and brain [10].

Biomedical signals such as ERG signals are challenging to interpret because they are the outputs of the physiological processes that reflect complex biological system's activity. Such signals are often non-stationary and hard to model because of randomness inherent in the signals varying from subject to subject. Feature extraction methods often extract the intrinsic characteristics of these signals. Extracted features often be used to develop methods that can provide an accurate diagnosis of the underlying pathology.

This review presents different ERG processing techniques and describes various signal processing methods to extract features from the human ERG signal. In this work, the methods exclusively applicable to the human ERG signals are compared and presented as summary tables. Each method's advantages and disadvantages will help physicians decide on feature extraction methods to better understand the retinal characteristics under normal and diseased conditions, and therefore help recommend additional clinical investigations to diagnose the underlying pathologies.

The associate editor coordinating the review of this manuscript and approving it for publication was Taous Meriem Laleg-Kirati.

There is no review article on feature extraction methods for ERG signal in the literature so far to the best of our knowledge. Review articles are readily available for ERG waveforms [11], [12], methods to diagnose retinal diseases using ERG in animals such as dogs [13], [14]. Also, detailed articles for specific retinal diseases using ERG [15], [16], and image processing-based techniques for diagnosing retinal diseases [17], [18] are available in the literature. However, no comprehensive review article, except a limited review for feature extraction for ERG signals using wavelets [19], exists in the area of feature extraction for the human ERG signals. This review article fills that gap in the literature.

II. METHODS

A. ERG SIGNAL AND RECORDING PROTOCOL

In this subsection, a brief overview of the ERG components and ERG recording protocol is presented. Retina approximately has 100 million rods and about 5-6 million cones. Thus, the rods are predominant in ERG responses [20]. The stimuli are used to record the ERG may stimulate different cells in different layers.

ERG is a short signal with a typical 200 milliseconds duration, in which the first 80 milliseconds contain most of the ERG components. One of the most important challenges in assessing the ERG is the differentiation of various cell responses. Based on the different responses obtained from the retina layers, ERG can be composed of multiple components. The two components that are most often evaluated in studies are the a- and b-waves. The a-wave is an initial negative deflection. The b-wave is a positive wave that directly follows the a-wave and usually has a significant positive amplitude [21], [22]. In addition to these two main components of ERG, there are three more components: the i-wave, which may originate from the OFF-pathway distal to retinal ganglion cells (RGCs) [23]; the photopic negative response (PhNR) that appears as a negative-going wave after the i-wave, which may be useful as a tool to monitor longitudinal change in RGCs function [24]; and the oscillatory potentials (OPs) which seem to be generated by the amacrine cells in the inner retina. The OPs usually appear after the b-wave and have more oscillations and less amplitude than other ERG components [25].

Studies showed that the photopic a- and b-waves could be found in the range of 20-40 Hz, which are defined as low-frequency components. The OPs are mostly observed within the 80-160 Hz range, known as high-frequency components of ERG [26].

International Society for Clinical Electrophysiology of Vision (ISCEV) introduced a protocol to standardize worldwide research on ERG analysis [27]. This protocol has been improved several times over the years, by adding more details to its different parts, especially in the stimuli and flashes related parts [28]–[30]. The standard clinical ERGs recording includes six responses based on the eye's dark and light-adaptation state and the different flash strengths: 1) dark-adapted 0.01 cd.s.m^{-2} ERG (b-wave: rod-initiated ON pathways); 2) dark-adapted 3.0 cd.s.m^{-2} ERG (a-wave: photoreceptor; b-wave: ON & OFF bipolar cells); 3) dark-adapted 3.0 cd.s.m^{-2} oscillatory potentials (ON & OFF pathways reflecting middle retinal layers & vascular function); 4) dark-adapted 10.0 cd.s.m^{-2} ERG (a-wave: photoreceptors; b-wave: predominantly rod bipolar cells (ON pathways)); 5) light-adapted 3.0 cd.s.m^{-2} ERG (a-wave: cones with post-receptoral ON & OFF pathways; b-wave: ON & OFF bipolar cells); and 6) light-adapted 30 Hz flicker ERG (cone systems with post-receptoral ON & OFF pathways) [27].

B. SIGNAL PROCESSING METHODS

The ERG analysis can generally be divided into four categories: time-domain, frequency-domain, time-frequency domain, and nonlinear and chaotic methods. Figure 1 presents the block diagram of various analyses for ERG signals based on the four categories and consolidates the number of papers available in the literature under each category.

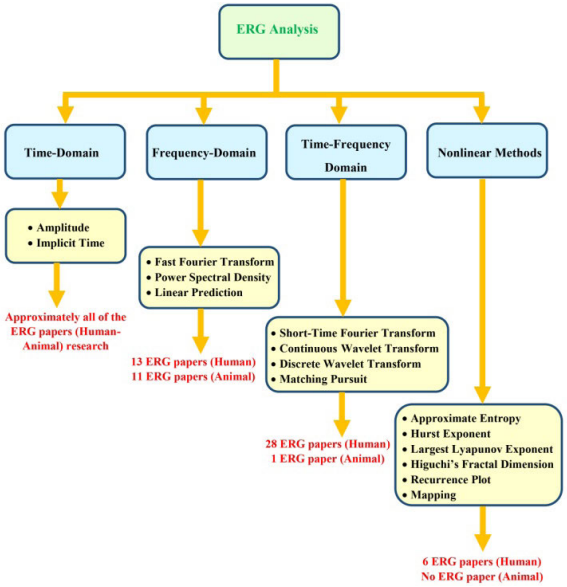

FIGURE 1. The block diagram of ERG studies is based on different analyses and the number of papers available under each category.

C. TIME-DOMAIN ANALYSIS

Time-domain features are extracted from a raw ERG signal in the time-domain. ERG analysis in the time-domain involves measuring two main parameters: the amplitude of each wave in the ERG signal and their implicit time, which is the time interval between the onset of the stimulus and each wave's peak. Amplitudes and implicit times are used to differentiate the response of a healthy subject from an unhealthy one or evaluate the process of retinal changes before and after a specific medication, surgical, or other treatment. Amplitudes and implicit times are the main parameters to assess the ERG changes, as almost all articles on ERG signal processing in the literature use these two parameters. Often, these parameters

are considered as benchmarks for comparing different signal processing methods. Since the number of studies on ERG analysis based on time-domain techniques is very high and the features extracted from time-domain analyses are numerous, we will avoid mentioning them. Although time-domain analysis is much prevalent in the literature, the time-domain features are sensitive to noise. Therefore, using time-domain features along with other domain features may alleviate issues posed by random noise. A common ERG is presented in Figure 2 to visualize the standard time-domain parameters measured from the ERG.

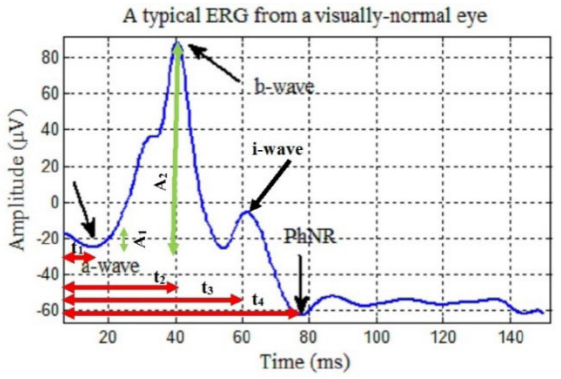

FIGURE 2. A normal ERG. Implicit time reflects the time between the initiation of the light stimulation and the peak of a- and b-waves. However, these parameters could be measured for other waves such as i-wave and PhNR. The a-wave amplitude is defined from baseline to the a-wave, while the b-wave amplitude is defined from the a-wave trough to the b-wave peak. These parameters are shown with appropriate variables, including t_1: a-wave implicit time; t_2: b-wave implicit time, t_3: i-wave implicit time; t_4: PhNR implicit time; A_1: a-wave amplitude, and A_2: b-wave amplitude.

D. FREQUENCY-DOMAIN ANALYSIS

A few studies have been performed to analyze the ERG in the frequency domain. Frequency analysis can recognize specific frequency changes in the ERG components [31]. Some of the frequency-domain-based techniques include the fast Fourier transform (FFT), power spectral density (PSD), and spectral estimation or linear prediction (LP).

1) FOURIER TRANSFORM

The Fourier analysis (FA) is a purely frequency-domain approach, which decomposes the signal or the given time series into its overall frequency components that build up that signal. The Fourier transform provides the weight that each frequency contributes to the original time-domain signal [32]. For the frequency-domain analysis, the signal is first converted from the time domain into the frequency-domain as follows:

$$F(\omega) = \int_{-\infty}^{+\infty} f(t)\, e^{-j\omega t} dt; f(t) = \frac{1}{2\pi} \int_{-\infty}^{+\infty} F(\omega) e^{j\omega t} d\omega \tag{1}$$

where, $f(t)$ is the time-domain signal, and $F(\omega)$ is the Fourier transform (spectrum) of $f(t)$. As seen in equation (1), the original signal can be recovered under certain conditions by the inverse Fourier transform. Moreover, discrete-time versions of both direct and inverse forms of the Fourier transform can be used. The Fourier transform in the discrete domain is achieved through the well-known fast Fourier transform (FFT) algorithm.

2) POWER SPECTRAL DENSITY

Characteristics of the ERG signal are obtained using the power spectral density (PSD) of the ERG samples [33]. The PSD is calculated by applying the Fourier transform of the estimated autocorrelation sequence [34]. The given data, $x(n)$ is divided into L smaller sequences, each of length M samples.

$$x_i = [x(n+iD), x(n+1+iD), \ldots, x(n+M-1+iD)], \quad n = 0, 1, 2, \ldots, M-1;\ i = 0, 1, 2, \ldots, L-1 \tag{2}$$

where, iD is the point of the start of the ith sequence. The modified periodograms are given in equation (3).

$$P_{xx}^{\approx(i)}(f) = \frac{1}{MU} \left| \sum_{n=0}^{M-1} x_i(n)\, w(n) e^{-j2\pi fn} \right|^2. \tag{3}$$

Here, in the window function, U indicates the normalization factor of the power and is selected such that:

$$U = \frac{1}{M} \sum_{n=0}^{M-1} w^2(n), \tag{4}$$

where $w(n)$ is the window function. The average modified periodograms give Welch's power spectrum [33]:

$$P_{xx}^{W}(f) = \frac{1}{L} \sum_{i=0}^{L-1} P_{xx}^{\approx(i)}(f). \tag{5}$$

The Welch periodogram provides the strength of the various frequency components in the ERG signal.

The non-parametric power spectrum estimation methods are relatively easy to compute using the FFT algorithm. One inherent assumption while using these methods is that the data record is long enough to obtain the needed frequency resolution. Also, these methods suffer from spectral leakage effects due to finite-length data records and may mask the weak signal components present in the signal. Furthermore, signals are assumed to be periodic, and the autocorrelation estimates are assumed to be zero after certain lags. ERG signals are short responses, and therefore many of the assumptions used in non-parametric estimation methods may not hold.

3) LINEAR PREDICTION

LP is a time series analysis method with different signal processing applications, such as modeling and feature extraction [35]. LP is a parametric spectral estimation technique, unlike PSD or the Fourier technique. LP is preferred when samples are not large enough to provide all the information needed for analyzing the ERG signal. If the series is adequately long, the FFT method can estimate the number of poles. LP optimally determines the dominant frequencies in

TABLE 1. Compilation of all frequency-domain studies applied on any ERG responses.

Year	Authors	Signal/ Stimulation	Feature/Method	# Subjects
1979	Gur et al. [37]	Corneal and non-corneal ERG	fast Fourier transform and linear prediction	4 Normal subjects
1980	Gur et al. [38]	Corneal ERG	fast Fourier transform and linear prediction	13 Normal subjects
1988	Van der Torren [39]	Oscillatory potentials of ERG	fast Fourier transform	NA
1990	Li et al. [40]	ffERG (scotopic and photopic)	Fourier spectrum	13 subjects with 23 Normal eyes
1998	Sieving et al. [41]	Flicker ERG	Discrete Fourier transform	NA
2012	Karimi et al. [31]	ffERG (scotopic and photopic)	Welch power spectral density	RP Group: 32 eyes Control Group: 22 Normal eyes.
2013	Chen et al. [42]	ffERG (scotopic and photopic)	fast Fourier spectrum (power spectrum)	8 Normal subjects
2014	Wood et al. [43]	focal cone ERG	Fourier spectrum (power spectrum)	Early age-related macular degeneration: 54 subjects Control Group: 54 Normal Subjects
2014	McAnany et al. [44]	A flicker of ffERG (photopic)	Fourier analysis	5 Normal subjects
2014	Gotzmann et al. [45]	Oscillatory potentials of ERG	fast Fourier transform	9 Normal subjects
2015	Pahl et al. [46]	Flicker ERG	fast Fourier transform	6 Normal subjects
2019	Zueva et al. [47]	Flicker ERG and PERG	Fourier Series	6 Patients with stage I and stage II primary open-angle glaucoma 6 Normal subjects

NA: Not available

the signals with short time-series, thus enabling simultaneous detection of frequency changes and data compression [36].

4) COMPARISON OF FREQUENCY-DOMAIN-BASED STUDIES

Table 1 represents a review of the human ERG evaluation based on frequency-domain analysis.

Bresli and Parker [37] recorded corneal and non-corneal ERG from healthy subjects. The signals were compared based on time- and frequency-domain analyses. The power spectra of both signals were evaluated using the FFT and LP methods. Except for amplitude differences, the two signals had identical a- and b-waves latencies and dominant power spectrum peaks. The authors reported that non-corneal ERG does not differ significantly from corneal ERG in time and frequency-domains.

Gur and Gath [38] analyzed the normal corneal ERG in the frequency domain using the FFT and LP methods. The authors identified four dominant frequencies (18, 79, 126, and 159 Hz) in dark-adapted stimuli of their analysis. They reported that low-frequency shifted to the higher frequency, and also the mid- and the two high-frequency components shifted to lower frequencies in light-adapt stimuli.

Gur and Zeevi [39] studied the OPs in diabetic retinopathy. To improve the accuracy of measuring the time-domain parameters, the ERG was first filtered with a finite impulse response (FIR) filter, followed by the FFT to separate the OPs from the a-wave. No more information about the filter was available. The dominant frequency determined the OPs powers in the FFT analysis. The results showed that even under pathological circumstances, a quantitative expression of the OPs is possible in diabetic retinopathy.

Van der Torren *et al.* [40] evaluated the dark- and light-adapted ERG for normal subjects utilizing the Fourier spectrum. They compared the coefficient of variation (CV), dominant power, and the OPs and time-domain parameters' dominant frequency. The CV is a criterion that is used as a ''measure'' for the dispersion of the frequency distribution. The higher the CV, the greater is the level of dispersion around the mean. The CV of these parameters was smaller in the light-adapted ERG compared to the dark-adapted ERG.

Li and Yuan *et al.* [41] studied the flicker ERGs of patients with retinal degeneration. They extracted in real-time six harmonic components using the discrete Fourier transform (DFT). Their primary purpose was to eliminate noise and large-amplitude artifacts. They used an analog-to-digital (A-D) digitizing board with eight switchable A-D inputs, which provides both eyes' recording simultaneously. A digital input-output line is pulsed at a 32-Hz rate by an on-board programmable clock to synchronize the flash stimulus precisely. Gaussian noise and artifact transients can be identified and removed through post-processing of the acquired data. If photoelectric artifacts were to occur from bright flashes striking the metal electrode, these would occur synchronously with the flash. It appears at the beginning of each response. If desired, the initial trace points could be nulled to zero to discard these initial A-D points for the measured duration of the artifact while saving the remainder of each response. The standard deviation of sequential intervals on a timeline of the sine component is generally used to identify quiet periods. This minimizes small-amplitude noise and improves the measurement consistency.

Karimi *et al.* [31] used frequency-domain analysis to study retinitis pigmentosa (RP) within affected subjects, especially to understand oscillatory and flicker responses. Their study used Welch's power spectral density estimation of the ERG

responses of RP and normal subjects. The peak frequency of the oscillatory and flicker response in RP subjects was higher compared to the normal subjects.

Sieving *et al.* [42] determined the frequency range of a-b-wave in the dark- and light-adapted normal ffERG. The time-domain parameters of a- and b-wave were estimated to determine the frequency range of a-b wave complex. Major frequency components were identified from power spectra using FFT. The frequency range of the dark-adapted a-b wave complex was significantly less than the light-adapted a-b wave complex. As the frequency of a-b waves was lower than that of Ops, a simple lowpass or bandpass digital filtering of the human ERG can separate a- and b-waves from the Ops.

Chen *et al.* [43] focused on analyzing focal cone ERG in early age-related macular degeneration. The ERG was recorded from patients with early age-related macular degeneration and healthy subjects as the control group. Conventional time-domain parameters and the frequency-domain power spectrum of the ERG were obtained for both groups. Time-domain parameters and power spectrum at 25 and 30 Hz frequency indicated significant differences between the two groups. The results confirmed the diagnostic potentials of both conventional times- and frequency-domain parameters. The low amplitude signals, such as focal ERG, could better be evaluated by frequency-domain parameters.

Wood *et al.* [44] evaluated the nature of changes in light-adapted flicker ERG's fundamental and harmonic components. The ffERG of visually normal subjects were studied using frequency analysis to obtain the amplitude and the three harmonic response components. Light adaptation affected the three harmonic components of flicker ERG differently, indicating ERG waveform changes during light adaptation.

McAnany *et al.* [45] studied the ON (b-wave)- and OFF (d-wave)- responses of the ffERG recorded from healthy subjects. They estimated time-domain parameters and used FFT to determine the dominant power and frequency. Four separated OPs were consistently phase-locked to the ON response (ON-OPs). The power of the ON-OPs peaked at shorter duration stimuli (<20ms). The dominant frequency (140 Hz) remained approximately constant for all durations. This study implied that OPs represent a mixed contribution from both the ON and OFF retinal responses in short-duration stimuli.

Gotzmann *et al.* [46] studied flicker ERG responses in normal subjects based on time- and frequency-domain analysis. They used the ISCEV standard protocol for ERG responses. Results showed that the determined frequencies related to flicker responses correlate with retinal functions and can potentially serve as a physiological indicator.

Pahl *et al.* [47] analyzed the signs of retinal pathologies using frequency response of photopic ERG and transient PERG in healthy subjects and patients with stages I and II primary open-angle glaucoma. They evaluated both signals based on the Fourier series and the spectra of different individuals. They used the coefficients of polynomials to smooth the resulted frequency response as a proposed feature for diagnosis. Each frequency response was divided into two frequency ranges, and an algebraic smoothing polynomial was applied to each of the responses in the frequency ranges. They used this modeling to identify the characteristics of retinal responses to the flicker- and pattern-stimulation.

Some other works focused on the ERG of animals with different stimuli based on the frequency-domain analysis and are as follows: Zueva *et al.* [48], Poppele and Maffei [49], Bach and Meigen [50], Bui *et al.* [51], Hancock and Kraft [52], Racine *et al.* [53], Rangaswamy *et al.* [54], Akula *et al.* [55], Dai *et al.* [56], Rocha *et al.* [57], Quintana *et al.* [58], and Dai *et al.* [59].

E. TIME-FREQUENCY ANALYSIS

The non-stationary and multi-frequency characteristics of biomedical signals confirm the need for a time-frequency domain method for analysis. The time-frequency analysis provides simultaneous interpretations in both time and frequency domains enabling explanation, presentation, and interpretation of ERG signals [60].

A review of the studies performed on a human ERG evaluation based on time-frequency-domain analysis is presented in Table 2.

1) SHORT-TIME FOURIER TRANSFORM (STFT)

STFT or the windowed Fourier transform is an essential technique for the time-frequency analysis, which obtains the Fourier transform of short segments of signals obtained by applying a window of a fixed length of time. Each short time segment can be assessed individually, and the frequency content of each segment can be displayed under the corresponding time segment.

The frequency resolution of the STFT depends on the length of the segment. Shorter segments in time will have a lower frequency resolution, and conversely for the longer duration segments [61]. The definition of the STFT is defined in equation (6).

$$STFT_x^{(w)}(\tau, f) = \int_{-\infty}^{+\infty} \left[x(t) .w(t-\tau) e^{-j2\pi ft} dt \right] \quad (6)$$

where, $x(t)$ is the signal, and $w(t)$ is the window function. The length and choice of the window dictate the content of the STFT. Windows minimize the effects of Gibb's phenomenon that leads to the creation of extraneous components in the spectrum of the signal studied. Gibb's phenomenon is due to the sudden truncation of the signal's frequency transformation. Different windows filter the extraneous components differently, which is generally referred to as side-lobe suppression. The length of the window dictates the frequency and time resolution of the STFT.

The STFT is usually displayed in two dimensions as the time axis x and the frequency axis y. As shown in Figure 3, the selected long window STFT (left figure) provides poor time resolution with a high-frequency resolution; however, a better time resolution (right figure) can be obtained with

TABLE 2. Compilation of all time-frequency-domain studies applied on any ERG responses.

Year	Authors	Signal/ Stimulation	Feature/Method	# Subjects
2000	Varadharajan et al. [72]	Scotopic ERG	DWT	37 Duchenne muscular dystrophy subjects Control Group:75
2005	Rogala et al. [74]	PERG	DWT	NA
2005	Penkala [75]	PERG	CWT	Retinal and optic Nerve diseases: 47 PERGs and 27 PVEPs Control Group: 60 Normal PERG waveforms; 60 Normal PVEPs
2007	Zhou et al. [76]	mfERG	MP	NA
2007	Varadharajan et al. [77]	Scotopic ERG	DWT	NA
2007	Penkala et al. [78]	PERG	CWT	102 Normal PERG recordings: < or = 50 years; > 50 years
2007	Barraco et al. [79]	Scotopic ERG	CWT	NA
2010	Barraco et al. [80]	Scotopic ERG	CWT	NA
2008	Miguel-Jimenez et al. [81]	mfERG	DWT	56 Open-angle glaucoma subjects Control group: 56 Normal subjects
2010	Miguel-Jimenez et al. [82]	mfERG	DWT	NA
2011	Miguel-Jimenez et al. [83]	mfERG	DWT	NA
2011a	Barraco et al. [84]	Scotopic ERG	CWT	NA
2011b	Barraco et al. [85]	Scotopic ERG	CWT	NA
2014	Barraco et al. [86]	Scotopic ERG	FA, PCA, and CWT	NA
2014	Dimopoulos et al. [87]	Scotopic and Photopic ERG	CWT	Normal subjects
2014	Nair et al. [88]	Scotopic and Photopic ERG, Flicker	CWT	95 subjects include Controls, CSNB, rod-cone dystrophy, and CRVO
2014	Gauvin et al. [89]	Photopic ERG	FA, CWT, and DWT	40 Normal subjects
2015	Miguel-Jiménez et al. [90]	mfERG	CWT	47 Glaucoma subjects Control group: 24 Normal subjects
2015	Kundra [91]	ffERG	DWT	10 Idiopathic Intracranial Hypertension subjects Control Group: 15 Normal subjects
2015	Gauvin et al. [92]	Photopic ERG	DWT	ON or OFF retinal pathway anomalies Control group: 25 Normal subjects
2016	Gauvin et al. [93]	Photopic ERG	DWT	21 Retinopathy subjects Control Group: 40 Normal subjects
2016	Alaql [94]	Photopic ERG	STFT, CWT, and DWT	One Normal subject
2016	Kundra et al. [95]	ffERG	DWT	20 Normal subjects
2017	Gauvin [96]	Photopic ERG	DWT	40 Normal subjects
2017	Brandao et al. [97]	mfERG	DWT	25 Primary open-angle glaucoma Control Group: 35 Normal subjects
2019	Hassankarimi et al. [98]	PERG	DWT	30 Early primary open-angle glaucoma Control group: 30 Normal subjects
2020	Behbahani et al. [99]	ffERG	CWT	17 CRVO subjects Control group: 17 Normal subjects
2020	Ahmadieh et al. [100]	ffERG	CWT	16 Nonproliferative diabetic retinopathy subjects Control group: 24 Normal subjects
NA: Not available				

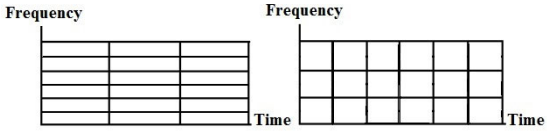

FIGURE 3. Time and frequency resolution of STFT.

reduced frequency resolution by choosing shorter windows. The signal amplitude is also displayed as a color indicator that distinguishes between high and low amplitude values. The main problem with STFT is the trade-off between time and frequency resolution and cannot be used for signals with non-constant sampling rates or when samples are missing [62], [63]. Figure 4 shows the STFT obtained for a healthy eye sample (top) and an eye with central retinal vein occlusion (bottom). The x-axis displays the time (ms), and the y-axis represents the frequency (Hz).

A comparison between the top and bottom figures shows that the normal subject had more low-frequency components before 100 ms. However, the CRVO patient's STFT had a shift toward high-frequency components.

2) WAVELET ANALYSIS (WA)

The wavelet transform is one of the time-frequency representation methods that has been widely used for analyzing ERG signals. Unlike STFT, WA does not have a fixed time and frequency resolution once the window length is

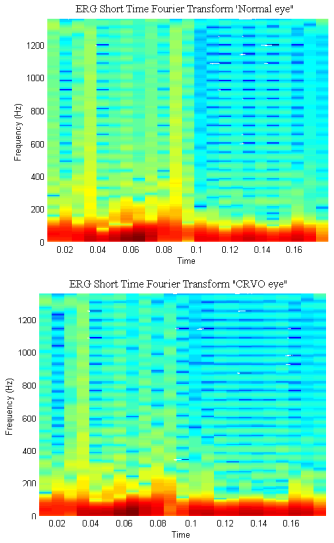

FIGURE 4. STFT was obtained for the healthy eye (top) and the eye with central retinal vein occlusion related to a sample patient (bottom).

selected. Wavelet transforms provide better frequency resolution at lower frequencies and good time resolution at higher frequencies. Unlike STFT, the time-frequency resolution of wavelet transform is generally logarithmic. WA is thus naturally suited for non-stationary signals such as ERG. WA includes two types of transforms, a continuous wavelet transform (CWT) and a discrete wavelet transform (DWT). Both CWT and DWT are used to analyze and display the timescale representation of a signal. Also, they decompose the signal into its multi-frequency (i.e., scale) components.

The CWT provides the correlation between the given signal $x(t)$ and a function referred to as wavelets. Wavelets are similar to windows in STFT, except that they either shrink or expand in length (often referred to as dilation or expansion, respectively). This is achieved through the parameter called "scale." The coefficients of the CWT are plotted against the scales of the transform. The wavelet coefficient equation is defined by the following equation [61]:

$$Cw(a,b) = \int_{-\infty}^{+\infty} x(t)\,\psi^*_{a,b}dt = \frac{1}{\sqrt{a}}\int_{-\infty}^{+\infty} x(t)\,\psi^*\left(\frac{t-b}{a}\right)dt \qquad (7)$$

where, $\psi^*(t)$ is the complex conjugate of the chosen wavelet, $Cw(a, b)$ are the wavelet coefficients, a is the scale parameter, b is the time localization parameter, and $\frac{1}{\sqrt{a}}$ is the energy normalization factor [64].

ERG signals can be decomposed using DWT. In DWT, the signal is convolved with discrete filters to achieve signal decomposition. The DWT can be realized as a filter bank of high pass and low pass filters along with up-sampling and down-sampling operations. The signal is divided into the low-band and high-band using a low pass and a high pass filter in the time domain. The convolution operation produces half the number of time samples as output. Generally, the low-band portion contains richer information about the signal. The procedure of producing low and high bands is repeated in the subsequent steps. The coefficient equation of the DWT is given by the following equation [61]:

$$DWT(j,k) = \frac{1}{\sqrt{2^j}}\int_{-\infty}^{+\infty} x(t)\,\psi\left(\frac{t-2^jk}{2^j}\right)dt. \qquad (8)$$

Equation (8) is obtained from the equation (7) by replacing a and with 2^j and b with 2^jk [65]. The schematic diagram of the decomposition of a signal using DWT is presented in Figure 5. As can be seen, DWT uses two filters, a low pass filter, and a high pass filter, to decompose the signal into different frequency scales.

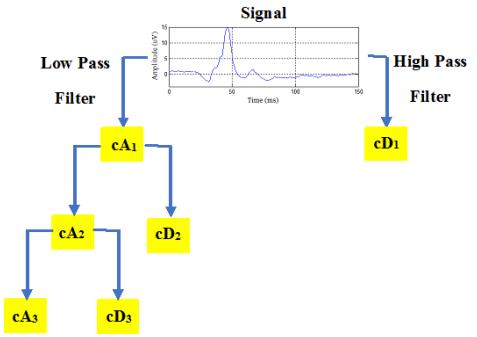

FIGURE 5. Signal decomposition using DWT.

The output coefficients of the low pass filter are called approximations (cA), while the output coefficients of the high pass filter are called details (cD). The approximation coefficients are related to low-frequency components of the signal. The detail coefficients are associated with the high-frequency components of the signal [61], [65].

3) MATCHING PURSUIT (MP)

Matching pursuit is an iterative algorithm that provides a promising time-frequency resolution for all frequencies. [66]. MP is more versatile than WA or STFT as MP adapts the window length to the time series' local features [67]. Therefore, the time-frequency resolution of MP is high and has been applied on different signals, such as Electroencephalogram (EEG), Electrocardiogram (ECG) [68]–[71]. Unfortunately, the application of MP for ERG signals is still in an incipient stage.

By performing an iterative procedure, MP finds a signal representation in a dictionary of functions, usually comprised of symmetric functions from the sine modulated Gaussian functions, such as Gabor. Using a time-frequency dictionary of Gabor functions, MP decomposes a 1D signal into a set of wavelet atoms adaptively. Based on the choice of time-frequency atoms like Gabor, the decomposition might have different properties. These waveforms are automatically selected to best match the signal structures. Assuming a set of functions (dictionary) as $D = \{g_1, g_2, \ldots, g_n\}$ with

$\|g_i\| = 1$. Note that $\|.\|$ will denote norm -2 in this paper unless specified otherwise. An optimal approximation for the signal can be obtained by minimizing the energy in the residual error ε which is obtained as the energy of the error between signal $f(t)$ and its representation obtained as a weighted sum of M waveforms, $g_\gamma(t)$. The residual error is defined as [68]:

$$\varepsilon = \left\| f(t) - \sum_{i=1}^{M} w_i g_{\gamma_i}(t) \right\| \quad (9)$$

where, w_i represents the weights.

The discrete Gabor dictionary can be defined as follows:

$$g_\gamma(t) = K(\gamma) e^{-\pi\left(\frac{t-M}{s}\right)^2} \sin(2\pi \frac{\omega}{N}(t-u) + \varphi) \quad (10)$$

where, N is the length of the signal for which the dictionary is constructed, $K(\gamma)$ is such that $\|g_\gamma\| = 1$, $\gamma = \{u, \omega, s, \varphi\}$ denotes the parameters of the dictionary's functions (time-frequency atoms), as time position, frequency position, scale, and phase, respectively.

4) COMPARISON OF TIME-FREQUENCY ANALYSIS-BASED STUDIES

Durka *et al.* [72] applied DWT in ERG signal processing. They studied Duchenne muscular dystrophy (DMD) patients based on DWT with Daubechies (db4) mother wavelet. They evaluated scotopic ffERG waveform using Mallat's multiresolution decomposition [73] to display the time-domain reconstruction of the wavelet coefficients obtained from seven different frequency bands of two groups as unhealthy (abnormal) and healthy (normal) subjects. The decomposition enabled the authors to differentiate unhealthy and healthy subjects at all frequency bands. It was concluded that the reconstructed DWT coefficients could represent physiological processes.

Mallat [74] applied the DWT with Daubechies mother wavelet to compare PERG responses of healthy and unhealthy subjects. The DWT features revealed more ability in differentiating normal and pathological PERG waveforms compared to the time-domain parameters. This can be attributed to extra information provided by the joint domain processing. The misclassification rate of time-domain parameters ranged between 55-60%, while 34-36% with the DWT.

Rogala and Brykalski [75] attempted to derive reliable features based on CWT to distinguish normal and abnormal PERG, as well as PVEP in some retinal and optic nerve diseases, including macular dystrophies–mainly Stargardt's disease glaucoma, ischemic optic neuropathies, and pituitary tumors. This study concluded that CWT is an efficient method to assess the latencies of the PERG waveforms. CWT provided good discrimination between normal and abnormal waveforms and enabled better features for the classification task.

Penkala [76] used the MP method to characterize OPs in the mfERG. They used the Gabor function to model the macular region of the retina. As a result, OPs were identified in frequency bands, including a high-frequency band around 150 Hz (that contributed to early Ops) and a low-frequency band peaking at approximately 80 Hz (that contributed to both early and late Ops).

Zhou *et al.* [77] showed the possibility to approximate the time-domain parameters for a-wave, b-wave, and also approximated at least one OP using the inverse DWT of scoptic ERG by reconstructing the signal using the wavelet coefficients. Daubechies mother wavelet was used in their study.

Varadharajan *et al.* [78] compared the results of time-domain analysis and CWT in determining the PERG parameters. The CWT method had more accuracy than the time-domain method and confirmed that it could differentiate normal and abnormal PERG, especially in the early detection of glaucoma.

Penkala *et al.* [79] focused on extracting information about the time-frequency characteristics of the human a- and b-wave, using WA. They choose Mexican Hat as the mother wavelet. According to their results, low-frequency components were e predominant (both in a- and b-waves), and their time distribution depended on luminance.

Barraco *et al.* [80] used WA to extract characteristics of the a-wave. Their work focused on the discrimination of two pathologies, achromatopsia and congenital stationary night blindness (CSNB), from healthy traces. Their results revealed that the number of dominant frequencies and their occurrence time in both studied diseases could represent retinal photoreceptors' status. Comparing selected pathological cases (achromatopsia and CSNB) with a normal control group showed that both disease's frequency components move toward lower values. The occurrence times of dominant frequencies had changed.

Barraco *et al.* [81] and Miguel-Jimenez *et al.* [82] and [83] conducted their research on analyzing mfERG based on DWT for normal subjects and glaucoma patients. They compared the results with traditional time-domain methods. Their results showed that DWT with Biorthogonal 3.3 (Bior3.3) mother wavelets are superior approaches to the traditional time-domain methods to detect glaucoma progression in patients.

Miguel-Jiménez *et al.* [84] continued their studies on a-wave to reveal this component's hidden characteristics and anomalies. They evaluated the time-frequency features of the a-wave, which were extracted from normal subjects and patients affected by achromatopsia. The patients with achromatopsia lose a part or total of their color vision. The results confirmed the existence of two or three frequencies that, in the pathological case, shift toward lower values and change their times of occurrence.

Barraco *et al.* [85] identified the stable time-frequency components of the a-wave, based on six representative values of luminance. The results showed three frequencies within the range of 20–200 Hz in the scotopic a-wave of normal ERG, in which the lowest frequency was attributed to the photoreceptors' accumulated activities. Other frequencies were

related to the response of the rods and the cones. This finding suggested that the CWT could be beneficial in the diagnosis of photoreceptor diseases.

Barraco *et al.* [86] compared the efficiency of three signal processing techniques: FA, principal component analysis (PCA), and WA, to discriminate subjects with retinal pathologies (such as achromatopsia and CSNB from healthy subjects). They reported that both PCA and FA techniques do not add clinically useful information to diagnose retinal pathologies. However, WA provided great potential for routine clinical examinations of patients.

Barraco *et al.* [87] studied OPs to determine whether age impacts rod- and cone-driven inner retina function. Dark- and light-adapted ERGs were recorded from healthy subjects. The time-frequency domain analysis was performed with the Morlet mother wavelet. In dark adaptation recordings, the decrease in the amplitude of OPs was confirmed with the selected method. The implicit times showed delay by the age of 40 years. WA defined the main frequencies in 150-155 Hz, which were unaffected by age. Most OPs created in light-adapted status showed delay by the age below 40 years. Two frequency bands, high frequency (135 ± 6 Hz) and low frequency (82 ± 7 Hz) were identified for Ops created by light-adapted ERG. By 60 years, there was a power reduction in the low-frequency band.

Dimopoulos *et al.* [88] attempted to automate the retinal disease diagnosis based on WA. The subjects from four different classes, namely healthy controls, CSNB, cone-rod dystrophy (CRD), and central retinal vein occlusion (CRVO), were assessed. The values of wavelet coefficients differed in the *a*-wave and *b*-wave amplitude of normal and pathological signals. Moreover, they applied the DWT with Haar wavelet to decompose the mfERG into three levels. They extracted the maximal wavelet coefficient from the full-field scotopic/photopic ERG and flicker mfERG. The results showed significant differences between the maximal approximation coefficient of the control and patient group. They concluded that DWT exposed subtle changes that were more sensitive than the traditional time-domain parameter. Therefore, significant diagnostic improvements were observed.

Nair and Joseph [89] compared the time-domain parameters of the photopic ERG using the frequency-domain (FA) and time-frequency domain (CWT and DWT). They evaluated the implicit time and amplitude measurements of the a- and b-waves, and the extracted features from FA, CWT, and DWT for normal ERGs. This study's results revealed the superiority of DWT features in recognizing the retinal diseases' decline over time. Changes in the ERG that were missed out in the time-domain analysis were captured by DWT features.

Gauvin *et al.* [90] investigated the application of WA in mfERG signals to diagnose glaucoma. The mother wavelet was Morlet. A group of patients was diagnosed with chronic open-angle glaucoma, and healthy subjects as a control group were considered. The glaucomatous regions were detected with high sensitivity (0.894). The specificity value (0.844) confirmed the accuracy in the healthy region detections.

Miguel-Jiménez [91] aimed to develop an approach to determine the frequency components and time range in the DWT that correspond to the PhNR of the ffERG. PhNR was evaluated as an index of RGCs function in idiopathic intracranial hypertension (IIH) patients. It was reported that the PhNR component of the DWT was reduced significantly in the patients with IIH compared to the subjects with visually normal controls. A good correlation was also seen between the PhNR assessed by DWT and that determined by conventional time-domain analysis.

Kundra [92] used DWT descriptors to study normal human photopic ERG evoked in response to a broad range of luminance intensities. Using the DWT descriptors, luminance-response curves were generated, revealing distinct luminance-dependence patterns. The various time-frequency components of the ERG were modulated differently by the stimulus luminance. Moreover, the ERG of patients affected with anomalies in the ON or OFF retinal pathway was assessed. The results indicated that well-defined time-frequency descriptors could be associated with the ON and OFF cone pathway functions.

Gauvin *et al.* [93] worked on photopic ERGs to investigate the possibility that the ERG signal is mostly composed of OPs. DWT analyzed the ERG of normal subjects and retinopathy patients. They reported that patients might present a wide range of OPs amplitudes. They confirmed the hypothesis that, in certain conditions, the photopic ERG could be comprised of high-frequency components.

Gauvin *et al.* [94] evaluated the photopic ERG signal using STFT, CWT, and DWT. The DWT-based evaluation provided more details regarding the frequency components in the ERG signal.

Alaql [95] studied the PhNR responses of ffERG in both time and time-frequency domains. The responses elicited by a long-wavelength pulse (3 cd.s.m^{-2}) were presented against a short-wavelength adapting field (12.5 cd.s.m^{-2}). Three to ten waveforms of each subject were analyzed using time-domain analyses and DWT to extract corresponding components of the PhNR. Three different measures of the PhNR include 1) amplitude at the PhNR trough; 2) amplitude at 72 ms following stimulus onset; and 3) energy in the 11 Hz, which corresponds to the PhNR were assessed. The results revealed that all selected metrics provide similar estimates of the PhNR.

Kundra *et al.* [96], in his doctoral thesis, tried to determine if advanced analytical approaches could extract additional useful physiological information from the photopic ERG and examined more than ten novels reproducible ERG descriptors derived from the DWT. Gauvin concluded that these descriptors were physiologically meaningful. The DWT approach described in this thesis can improve the ERG sensitivity and specificity of retinal disease diagnosis based on the characteristics of photopic ERGs for a given disease.

Gauvin [97] worked to improve the evaluation of two flashes mfERG in open-angle glaucoma using DWT with Daubechies mother wavelet. The results indicated an improvement in mfERG glaucoma diagnosis based on WA, especially when combined with ganglion cell–inner plexiform layer.

Brandao *et al.* [98] used the DWT and descriptors of PERG waveforms to determine early primary open-angle diagnosis glaucoma characteristics. They used the Daubechies filter as the mother wavelet and showed that DWT could quantify PERG responses accurately.

Karimi *et al.* [99] determined the effect of CRVO on PhNR and RGCs performances based on CWT. The PhNR of ffERG of patients was compared to the fellow normal eyes. Additionally, the standard time-domain analyses of the PhNRwas conducted. The main frequencies and their occurrence time were obtained using CWT. All a-wave, b-wave, and PhNR amplitudes of CRVO eyes showed a significant reduction compared to those of the fellow eyes. CWT was successful in quantifications of PhNR responses.

Ahmadieh *et al.* [100] compared time and time-frequency domain characteristics of ERG in nonproliferative diabetic retinopathy patients. The implicit times of b-waves in the dark-adapted 10.0 and light-adapted 3.0 were significantly increased in the patient group. The amplitudes of a- and b-waves had a decreased value in dark-adapted 10.0 and light-adapted 3.0 ERG of the non-proliferative group considerably. The results confirmed that the time and time-frequency parameters of photopic and scotopic ERGs could be good indicators for diabetic retinopathy.

Ahmadieh *et al.* [101] used WA to reveal the dynamics of rat OPs. Table 2 describes all the time-frequency domain studies applied to ERG responses.

F. NONLINEAR METHODS

One of the essential characteristics of natural systems is their nonlinearity and the ability to produce complex behaviors. Complexity is due to the interactions that each natural system has with its surroundings and other systems. In addition to the time-domain, frequency-domain, and time-frequency domain analysis of the ERG, some features have been used in a limited number of articles related to ERG signal processing. These parameters include approximate entropy (ApEn), largest Lyapunov exponent (LLE), Hurst exponent (HE), Higuchi fractal dimension (HFD), and Recurrence plot.

1) APPROXIMATE ENTROPY

ApEn is a nonlinear parameter that exhibits the complexity of a time series. The more complex the time series, the higher the Forte [102]. ApEn is a measure of irregularity in time-series, which is derived by comparing the similarity patterns of template vectors. It measures the unpredictability of fluctuation patterns. Therefore, the more repetitive the patterns are, the more predictable the time series are. Assuming a time-series of data as u(1), u(2), . . . , u(N), based on the measurements that are equally spaced in time, a sequence of vectors can be formed as x(1), x(2), . . . , x(N − m + 1), and in R^m defined by x (i) = [u (i) , u (i + 1) , . . . , u(i + m − 1)]. Next, for each i, 1 ≤ i ≤ N − m + 1 t he self-similarity of the template vector $u\,[i]$ with a tolerance r, can be defined as:

$$C_i^m(r) = \frac{1}{N-m+1}\sum_{j=0}^{N-m}\Theta(r - \|u\,[i] - u[j]\|_\infty) \quad (11)$$

where, Θ(x) is the Heaviside step function, i.e., Θ(x) is one when x ≥ 0, and zero otherwise. When x is mostly self-similar, then $u\,[i]$ and $u[j]$ sequences are very close and thus C_i is high. The ApEn is defined in equation (12) [103]:

$$\begin{aligned}\text{ApEn (X, m, r)} = &\frac{1}{N-m+1}\sum_{j=0}^{N-m}\log C_i^m(r)\\ &-\frac{1}{N-m}\sum_{j=0}^{N-m-1}\log C_i^{m+1}(r). \quad (12)\end{aligned}$$

2) HURST EXPONENT

HE is an index of long-range dependency, which indicates a degree of time-series tendency. A time series of X as a signal with a full length of N is divided into D numbers of shorter time series with length n, where D is an integral divisor of N. For each of the subseries $X_m, m = 1, 2, 3, \ldots, D$, the following steps are performed [104]:

Step 1: Find the mean, μ_m and the standard deviation, σ_m.

Step 2: Remove the mean from the series and form the mean adjusted series, X'_m. Let the elements of this series be denoted by $x'_{i,m}$.

Step 3: Form the cumulative time series, $Y_{i,m}$, given by, $Y_{i,m} = \sum_{j=1}^{i} x'_{j,m,}$, $i = 1, 2, \ldots, n$.

Step 4: Find the range R_m of the cumulative series, that is

$$\begin{aligned}R_m = &max(Y_{1,,m}, Y_{2,m}, Y_{3,m}) \ldots\ldots Y_{n,m})\}\\ &-min(Y_{1,,m}, Y_{2,m}, Y_{3,m}) \ldots\ldots Y_{n,m}). \quad (13)\end{aligned}$$

Step 5. Rescale the range by dividing it by the standard deviation, σ_m that is found $(R/S)_m = R_m/\sigma_m$.

Once all the rescaled ranges are calculated for all the D series of length n, calculate the mean value of the rescaled ranges for the series of length n as follows:

$$(R/S)_n = \frac{1}{D}\sum_{m=1}^{D}(R/S)_m. \quad (14)$$

The HE is estimated as the slope of the best fit line for the plot of $log\left((R/S)_n\right)$ as a function of n.

3) LARGEST LYAPUNOV EXPONENT

Nonlinear dynamic systems are highly sensitive to the initial conditions. The smallest change in system state variables at one point will cause substantial changes in the system's future behavior. Lyapunov exponent, λ, is an index to evaluate the chaos of a nonlinear dynamical system. It measures the rate at which the trajectories separate from each other. It gives dynamic information about attractors. LLE measures provide the average rate of convergence or divergence of nearby trajectories in phase space. A pair of nearest neighbors $[x\,(i)\,, x\,(j)]$, starting close to one another in a chaotic system,

diverges approximately at a rate given by the LLE λ [105]. To obtain LLE, consider:

$$d_j(i) \approx d_{j0} e^{(i\Delta t)} \tag{15}$$

where, $d_j(i)$ is the Euclidean distance after i time steps. The sampling rate of the time series and the initial pair separation are Δt and d_{j0}, respectively. Solving the equation (15) by taking the logarithm of both sides, the LLE can be calculated as follows:

$$\lambda \approx \frac{1}{i\Delta t} \ln\left(\frac{d_j(i)}{d_{j0}}\right). \tag{16}$$

A positive Lyapunov exponent is a good indicator of the chaotic nature of a system.

4) HIGUCHI's FRACTAL DIMENSION

HFD is considered a nonlinear measure of waveform complexity in the time domain. Discretized signals could be analyzed as time sequences x(1), x(2),..., x(N). Starting with a time sequence, a new self-similar time series x_k^m can be calculated as given in equation (17) [106]:

$$x_k^m = x(m), x(m+k), x(m+2k), \ldots, x \times \left(m + \text{int}\left[\frac{N-k}{k}\right]k\right), \text{for } m = 1, 2, \ldots, k \tag{17}$$

where, m is the initial time; k is the time interval, $k = 1, \ldots, k_{max}$; k_{max} is a free criterion, and int(r) is the integer part of the real number r. HFD is highly dependent on the value of k_{max}; therefore, k_{max} plays a crucial role in HFD estimation. "The length" of the curve $L_m(k)$ is determined for each of the k time series x_k^m as follows:

$$L_m(k) = \frac{1}{k}\left[\left(\sum_{i=1}^{\text{int}\left[\frac{N-k}{k}\right]} |x(m+ik) - x(m+(i-1)k)|\right)\frac{N-1}{\text{int}\left[\frac{N-k}{k}\right]K}\right] \tag{18}$$

where, N is the length of the main time-series X and $\frac{N-1}{\left\{\text{int}\left[\frac{N-k}{k}\right]K\right\}}$ is a normalization factor. The mean value of the curve length $L(k)$ for each $k = 1, \ldots, k_{max}$ can be defined by averaging $L_m(k)$ for all m as:

$$L(k) = \frac{\sum_{m=1}^{k} L_m(k)}{k}. \tag{19}$$

An array of mean values $L(k)$ is thus obtained, and the HFD is estimated as the slope of the least-squares linear best-fitting procedure, which includes a plot of $\ln(L(k))$ versus $\ln(1/k)$:

$$\text{HFD} = \ln(L(k))/\ln(1/k). \tag{20}$$

5) RECURRENCE PLOT

A recurrence plot is a two-dimensional plot that enables the visualization of higher-dimensional phase spaces and is used to characterize the underlying dynamics. In a recurrence plot at coordinates (i, j), black dots are plotted when recurrence events ($R_{i,j} \equiv 1$) occur, and white dots are plotted for nonevents ($R_{i,j} \equiv 0$) [107].

$$R_{i,j} = \begin{cases} 1: & \left\|\vec{x}_i - \vec{x}_j\right\| < \varepsilon \\ 0: & otherwise. \end{cases} \tag{21}$$

To construct the recurrence plot, a symmetrical $N \times N$ array, called recurrence matrix R is computed as follows [107], [108]:

$$R_{i,j}(\varepsilon) = \Theta(\varepsilon - \left\|\vec{x}_i - \vec{x}_j\right\|) \tag{22}$$

where, $\vec{x}$ contains the N intended states, $\Theta(x)$ is the Heaviside function, ε is the threshold distance, and $\|.\|$ is a norm.

6) ANGLE CRITERION

ERG is assumed as a time series, which represented by X, and a map is constructed using the relation between each of the points in the time series with a meantime series, $\bar{X}$:

$$mean(X) = \bar{X} = \frac{1}{n}\sum_{i=1}^{n} X_i. \tag{23}$$

So, mapping consists of all below pairs:

$$\left(X_i, \left(\bar{X} - X_i\right)^2\right), \quad i = 1, 2, 3, \ldots, n \tag{24}$$

where, n is the total number of samples in time-series such as ERG.

By evaluating the distribution of points in this new arrangement, a second-degree polynomial equation in the form of $Y = \alpha x^2 + \beta x + \gamma$ is obtained from this map, which $Y = \left(\bar{X} - X_i\right)^2$. The three principal parameters of the parabolic curve, α, β, and γ are estimated.

The pairs of $\left(X_i, \left(\bar{X} - X_i\right)^2\right)$ form a new arrangement of the points. The ERG comprises positive and negative amplitudes. Therefore, based on equation (24), some parts of the signal will accumulate on the parabola's left or right sides [109].

A criterion for showing the arrangement of points on the parabola's right or left side is the angles made by drawing a line from the beginning to endpoints distributed on the parabolic and horizontal axis. For the angles of less than 90 degrees, the accumulation of points on the right side is more. In other words, there are more positive waves with higher amplitudes. For the angles below 90 degrees (negative values), the accumulation is drawn to the left side of the parabola, which indicates the appearance of the negative amplitude waves [109]. The angles close to zero confirm the balance distribution based on positive and negative waves. Figure 6 represents the mapping, distribution of points on the curve, and the angle θ. The angle θ is calculated based on equation (25).

$$\boldsymbol{\theta = arctang \frac{opposite(a\ or\ b)}{adjacent}} \tag{25}$$

TABLE 3. Comparison of all nonlinear studies applied on any ERG responses.

Year	Authors	Signal/ Stimulation	Feature/Method	# Subjects
1998	Crevier et al. [110]	ffERG	Nonlinear feedback-Period doubling	NA
2008	Etter et al. [111]	ffERG	HE	10 Glaucoma subjects Control group: 10 Normal subjects
2014b	Nair [112]	ERG	HE, LLE, HFD, ApEn, and recurrence plot	35 CSNB, 15 RP, 35 CRD subjects Control Group: 15
2014	Molaie et al. [113]	ERG	Black-box modeling-Period doubling	NA
2017	Sarossy et al. [114]	Scotopic ERG	Entropy	21 Glaucoma patients Control group: 18 Normal subjects
2020	Sefandarmaz et al. [109]	Scotopic and Photopic ERG	ApEn, HE, and angle criterion	17 CRVO eyes with their fellow eyes as Control group

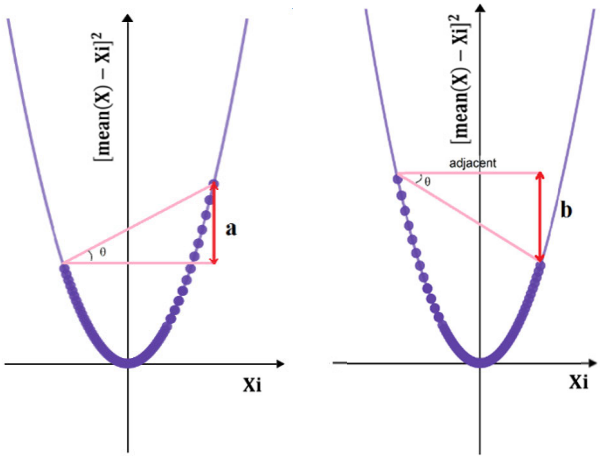

FIGURE 6. Angle Index in the parabolic map, (LEFT) the accumulation of points on the right sides (positive θ), (RIGHT) collection of points on the left sides (negative θ) [109].

7) COMPARISONS OF STUDIES IN NONLINEAR METHODS

Sefandarmaz *et al.* [110] studied human visual systems' disorders using periodic flashes of light and identified that ERG exhibits a periodic doubling behavior. From the nonlinear dynamical system theory, it is understood that periodic-doubling indicates the onset of chaos. This study confirms the existence of chaotic behavior in flicker ERG.

Crevier and Meister [111] determined the potential of chaotic behavior in normal and glaucoma subjects based on ffERG patterns. Ten normal subjects and ten patients with glaucoma were evaluated. The HE trended lower in glaucomatous patients (median = 1.8) compared to the normal patients (1.9) ($p = 0.15$). The results indicated that the ffERG of glaucomatous patients appeared to exhibit less chaotic behavior, which corresponds with the hypothesis that healthy subjects are more complex systems with more chaotic dynamics; however, the difference was not statistically significant.

Etter *et al.* [112] studied the ERG signal's chaotic aspect in the retinal disease, including CSNB, RP, CRD, and a control group. Nonlinear parameters like HE, LLE, HFD, ApEn, and recurrence plots were analyzed for these four groups. The results revealed that HE and ApEn are higher for controls than for the retinal disease groups. However, LLE showed no different variations for the three groups of retinal diseases. The recurrence and phase-space plots showed change among all three analyzed groups. It was concluded that ERG complexity in control groups was higher than retinal diseases with $p < 0.05$.

Nair and Joseph [113] worked on flash frequency and contrast as effective parameters in the ERG recordings. They reported that these parameters significantly impact the recorded signals and lead to bifurcations, indicating chaotic behavior.

Molaie *et al.* [114] explored subtle timing changes in the ERG of glaucoma patients based on the entropy features. They calculated the entropy of ERG signals within a sliding window and then used Kolmogorov–Zurbenko adaptive (KZA) filter to detect the peaks and the timing of entropy changes. The results indicated an earlier rise in entropy in glaucoma patients, confirming this approach's potential to diagnose glaucoma.

Heunis *et al.* [109] introduced a nonlinear criterion to evaluate the ERG in patients with CRVO. Also, some other nonlinear features such as HE and ApEn were extracted from the control and CRVO group. The parabolic map and proposed criterion (θ angle) provided successful results in differentiating the groups.

Table 3 describes all the nonlinear studies applied to ERG responses.

III. DISCUSSION

The ERG signal involves recording retinal cells' electrical activity after stimulation, which is widely used to detect different retinal layers' functions. The ERG signal is a short signal that contains many components working at the same time. The short length of ERG and its complex nature and nonlinear dynamics make it challenging to select an appropriate analysis method. A review of articles written in ERG signal processing shows that the standard criterion for evaluating retinal cells' function in various layers is assessing the amplitude and implicit time of known waves in this signal. Almost all articles on the analysis of ERG have reported processing in the time domain.

ERG was also analyzed using a frequency-domain approach. Of course, the number of articles written in non-time-domain analysis of the ERG is far less than other vital signals, such as ECG and EEG signals. Simply twelve articles on human research and ten articles in animal research are based on the ERG frequency-domain analysis in the literature. The human-related papers that analyzed ERG in the frequency domain used the FFT, PSD [31], [37]–[47], and two of them utilized LP [37], [38]. It is hard to compare studies because of the variations in the ERG components from different cells and retinal layers and various retinal diseases. Only two articles [85], [89] in the ERG literature have conducted studies under the same stimulation and considered the same disease, and compared the findings. Research articles show a great deal of diffusion between research methods and subjects in the field of retinal diseases, and non-time-domain methods have not been standardized and generalized. However, these methods have either improved or confirmed the same results in any research that has used time-domain analysis.

The frequency-domain-based approaches reduce or eliminate noise from the ERG signal [32], [35]. ERG is highly susceptible to noise, which can affect the results of the time-domain parameters. By removing noise effects, estimating parameters containing significant features becomes more robust, and better classification performance can be achieved. There is a great deal of variation in ERG-based research that has used the frequency domain approach, and various retinal diseases have been studied under different conditions. However, the research focused on the frequency domain had a common strategy: most of them focused on the OPs component [31], [40], [41], [43], [46]. A reason for choosing OPs is that they have shorter amplitudes than all other ERG components [25]. Therefore, it is challenging to distinguish OPs in terms of time-domain parameters.

FFT is a helpful tool to analyze stationary, infinite duration, and periodic signals. However, most of the biological signals, including the ERG, are non-stationary. FFT is more appropriate for narrowband signals, while ERG is not a narrowband signal. If research is concerned with examining specific waves or components of the ERG, then the ERG's high and low frequencies must be separated. The narrower the frequency range considered, the higher the chance of success is. In the case of a- and b-waves, the frequency range is determined based on the FFT method. These two waves were located in a narrowband range between 15-40 Hz, and as expected, the results showed a correlation with retinal functions [43].

Although the short amplitude of OPs results in better frequency-domain analysis than the time-domain method, such analysis brings a severe challenge due to the required preprocessing. The OPs should be extracted using a bandpass filtering technique to remove the low-frequency components of the ERG. On the other hand, bandpass filtering might introduce distortions such as phase lag, ringing artifacts, or attenuation of OPs amplitude. These distortions can go as far as even creating artificial OPs [29, 89]. Since the FFT determines all frequency components' power in a signal, these distortions can potentially lead to misinterpretations [89], [91].

Another problem with FFT is the lack of time localization, which means that the power spectrum cannot provide information about specific signal frequencies. STFT was proposed to analyze small sections of the signal by windowing [115], [116]. STFT provided the basis for time-frequency domain analysis. Although the STFT can add some temporal resolution to the FFT and reveal the signal's time and frequency information, it has low temporal resolution if the selected analysis window's length is long. Therefore, the biggest challenge of STFT is the requirement to adjust the length of the windows case-by-case to avoid resolution problems. The STFT cannot simultaneously capture both short-duration-high-frequency and long-duration-low-frequency information [96].Smaller window size leads to better time-resolution and decreases the number of discrete frequencies represented in the frequency domain [110]. Gauvin [94] compared the results of the STFT with other time-frequency methods and found out that WA provides the full potential of differentiating the ERG components.

The main challenge in the papers that used WA is the selection of the mother wavelet. The related articles still seem not to agree on the best mother wavelet to match the ERG signal. The mother wavelets reported in the literature include ''Daubechies'' wavelets [71], [76], [92], [97], the ''Haar'' wavelet [87], [88], and the ''Mexican hat'' [84]–[86]. Miguel-Jimenez *et al.* [83] have successfully applied DWT to the global flash mfERG response in advanced glaucoma but did not specify mother wavelets. Finally, they found that the Biorthogonal 3.1 (Bior3.1) mother wavelet had the best performance in visual comparison. CWT using the Morlet wavelet provided acceptable results in [89]. Variations in the selection of mother wavelets can somehow be one of the WA method's benefits as some may more suitably describe the features of the signal than others. This benefit contrasts with FA expressed as a sum of sines and cosines [96].

The use of WA has advantages over other frequency-domain methods. It has a varying window size, being broad at low frequencies and narrow at high frequencies. Moreover, WA is better suited for the analysis of sudden and transient signal changes. It could be an excellent method to analyze irregular data patterns, such as impulses existing at different time instances [35].

Unlike STFT, which uses a fixed window, CWT uses a varying window approach. To analyze the low-frequency spectral components in the signal, it uses the longer window and shorter windows to analyze the high-frequency spectral components in the signal. This makes the CWT a better approach to analyze ERG signals. Most biological signals have low-frequency components that spread over long durations and high-frequency components that spread over short durations [94]. The literature review showed that some articles had taken advantage of CWT. Most of these papers have examined the PERG signal, which is a low-frequency signal [114] and determines the function

TABLE 4. Advantages and disadvantages of ERG analysis methods.

Method	Advantage/Disadvantage
FFT	**Advantages:** Good tool for stationary signal processing; Appropriate for the narrowband signal; **Disadvantages:** Cannot analyze short durations signals or nonstationary signals; Poor frequency estimation under low signal-to-noise ratios; rectangular window introduces Gibbs's effect while tapered windows cause loss of power at the edges and also broaden the spectrum. cannot reveal the localized spikes
Linear prediction	**Advantages:** Possibility of simultaneous detection of frequency changes and data compression **Disadvantages:** Not applicable when the signal becomes nonstationary.
CWT	**Advantages:** A varying window size, high-frequency resolution at low frequencies, and high time resolution at high frequencies; possibility to obtain better information in abrupt frequency changes and is suitable for extracting features from nonstationary signals. Provided redundant decomposition and therefore ideal for extracting features of signals that have variations within subjects. **Disadvantages:** Choice of appropriate mother wavelet is needed for good feature representation.
DWT	**Advantages:** Capable of providing reasonable time and frequency resolution simultaneously. **Disadvantages:** Feature extraction depends on appropriate mother wavelet; generally shift variant; not suitable for signals that have quadratic frequency variations, and does not provide phase information
STFT	**Advantages:** Possibility to analyze transient harmonics. Can handle noisy signals. **Disadvantages:** Window size fixes the resolution in time and frequency; cannot provide a good time and frequency resolution simultaneously; cannot provide features for short-duration signals.
ApEn	**Advantages:** Good for small data samples ($n < 50$ points); can be applied in real-time; Less sensitive to noise. **Disadvantages:** Strongly dependent on the signal length, often lower than expected for short records; Lacks of relative consistency.
HFD	**Advantages:** HFD could be applied to nonstationary, stationary, stochastic, and deterministic, as well as synthetic or natural signals. HFD is relatively independent of the length of the nonstationary signal. **Disadvantages:** Sensitivity of HFD to noise and frequency bands; a relatively narrow interval of HFD values means similar HFD values could characterize various signals.
Recurrence plot	**Advantages:** Can be used with short and nonstationary data **Disadvantages:** The selection of recurrence thresholds is adhoc.
Matching Pursuit	**Advantages:** High time-frequency resolution; provides a good parametric description of signals, including its frequency, amplitude, latency, time span, and phase. Works well with shorter signals. **Disadvantages:** Features and decomposition depend on the dictionary's atoms; can lead to non-unique decompositions. Decomposition for larger signals is computationally burdensome.
Angle Criterion	**Advantages:** Can extract the dynamics of very short signals and detect small changes in the signal. **Disadvantages:** It only works in a good signal/noise ratio and fails when the signals are noisy.

of RGCs [75], [78], [82], and have reported good results. Barraco *et al.* worked on ERG based on CWT in five papers and mainly studied the a-wave, a low-frequency component [79], [81], [84]–[86].

The remaining time-frequency domain papers available in the literature were based on DWT. Both CWT and DWT methods have their advantages and disadvantages. CWT is more reliable than DWT, as it can extract all information without down-sampling. However, CWT needs more computation, which leads to a slower process compared to DWT.

Moreover, CWT is highly redundant, which is beneficial from one perspective and a curse from another perspective. As it is redundant, no information gets lost, unlike DWT. In DWT, there is a possibility to lose some information if the right level of decomposition is not chosen. Two significant factors in WA analysis that should be considered are the type of wavelet and the decomposition [115].

Heisenberg's uncertainty principle dictates that it is impossible to determine an oscillatory component's exact frequency and position in the same representation of a concise portion of the signal. Therefore, a signal has a high localization in time or frequency, but not both [116], [117]. The OPsas high-frequency components are associated with a signal over an acceptable time scale, which allows the information extraction regarding their timing to be preserved at the cost of a lower spectral resolution. The low-frequency components such as a- and b-waves are associated with a coarse time scale, which leads to imprecise temporal resolution. The exact timing of the oscillation remains uncertain.

For the evaluation of small bandwidth changes, a high spectral resolution is required. However, the detection of large bandwidth changes requires less frequency resolution. The bandwidth of a- and b-waves comprises the frequency range between 15-40 Hz, i.e., a 25 Hz bandwidth. The OPs frequency band covers 75-200 Hz, which means the bandwidth is approximately 125 Hz. Therefore, a- and b-waves have smaller bandwidths compared to OPs. Analysis using the DWT could provide the necessary high spectral resolution for a- and b-waves and less spectral resolution of the OPs [96]. ERG's low-frequency components (including a-wave, b-wave, and PhNR) were studied using DWT in different retinal diseases [88], [89], [91], [95]. The results of all research were satisfactory compared to the time-domain analysis.

Only one work [76] had an analysis based on the MP method among the ERG articles. MP method has high time-frequency resolution and a structure with local self-adapting capability. This paper was successful in finding the OPs components, high and low-frequency OPs. MP method is not affected by noise, and therefore, higher quality characteristics can be obtained. Both of these advantages are crucial for ERG analysis. Moreover, MP can overcome the shortcomings

of FA, STFT, and WA by decomposing the signal so that waveforms can better match the signal structure [118].

Physiological signals exhibit complex behavior that reflects the nonlinear dynamic properties of biological systems. Nonlinear feature extraction methods and chaos theory have many applications in evaluating vital signals [105], [119]–[121]. Although linear methods are mostly used in analyzing ERG signals, nonlinear features also show aspects that cannot be investigated using linear methods. However, published works in this field are still deficient [109]–[113]. Using nonlinear tools to represent chaotic behaviors can be a good choice for discovering the ERG signal's nature.

The nonlinear and chaotic methods used to analyze ERG signals have good potential to extract useful features. These features can show the underlying dynamics within the retinal system well. All linear methods reviewed in this paper required windowing. Windowing had its issues as different windows with window length impacted the time and frequency resolutions. Nonlinear methods do not require windowing and therefore are devoid of such limitations. However, the computational requirements of nonlinear methods may be higher than the linear methods such as WA, or FA Lyapunov exponent requires all the states to evolve to obtain the divergence of the trajectories and, therefore, may need time to execute. The short length of the ERG signal can be a challenge in such computations. In this case, the Lyapunov exponent can be used as an index to confirm or reject the significant changes in different states.

One of the critical points observed in the ERG processing methods is the lack of geometric analysis and different mappings, such as angle criterion [114]. The angle criterion s based on the parabolic curve has the potential to differentiate CRVO patients from normal. This method can be further investigated for other types of retinal diseases. Due to the short length of ERG and the overlap of the different layer's functions, the methods that extract the information of signals based on point arrangements in time series can better evaluate ERG changes.

As a general summary of the methods used to analyze this signal, Table 4 summarizes each method's advantages and disadvantages for ERG analysis. The items presented in this Table are centered on the ERG signal and may not necessarily be considered as an advantage or a disadvantage for other biological signals. Moreover, the expression of merit and demerit in this Table is not based on comparing each method. Each method is judged separately from the perspective of its ability to analyze the ERG signal.

Considering the current review and the selection of different approaches in published articles, it seems that each method has some ability to extract information from the ERG signal.

Given the nature of the ERG signal, with a good understanding of the potential of the various methods described in this review, an appropriate choice of feature extraction may be possible when the type of retinal disease is known a priori.

IV. CONCLUSION

In this article, we have reviewed the methods used to process and extract features of the ERG signal. We have categorized most of the ERG signal processing methods that identify most information from the retina in normal subjects and subjects with different retinal diseases.

Although the time-domain parameterization approach has been well-known as a standard method in all the reviewed articles, it has drawbacks. Therefore, alternative methods have been proposed to overcome the drawbacks of time-domain approaches. Most papers showed the superiority of frequency-domain and time-frequency methods over the time-domain parameters used for ERG analysis. Interestingly, despite ERG being a short-duration signal, parametric spectral estimation methods have not been widely used.

Given the complex characteristics of ERG signals, the nonlinear and chaotic methods that illustrate the system's complexity are suitable for thoroughly analyzing and distinguishing between retinal layer performances. Due to diversity in the retinal layers and differences in the cell's function, a single universal feature extraction approach may not be possible. In some cases, a combination of methods might be a better choice.

V. ABBREVIATIONS

ApEn: Approximate Entropy; **CRD:** Cone-Rod Dystrophy; **CRVO:** Central Retinal Vein Occlusion; **CSNB:** Congenital Stationary Night Blindness; **CV:** Coefficient of Variation; **CWT:** Continuous Wavelet Transform; **DMD:** Duchenne Muscular Dystrophy; **DWT:** Discrete Wavelet Transform; **ECG:** Electrocardiogram; **EEG:** Electroencephalogram; **EMG:** Electromyogram; **ERG:** Electroretinogram; **FA:** Fourier analysis; **ffERG:** full-field Electroretinogram; **FFT:** fast Fourier Transfor; **FIR:** Finite Impulse Response; **GCIPL:** Ganglion Cell–Inner Plexiform Layer; **HE:** Hurst Exponent; **HFD:** Higuchi Fractal Dimension; **IIH:** Idiopathic Intracranial Hypertension; **ISCEV:** International Society for Clinical Electrophysiology of Vision; **LLE:** Largest Lyapunov Exponent; **LP:** Linear Prediction; **KZA:** Kolmogorov–Zurbenko Adaptive; **mfERG:** multi focal Electroretinogram; **MP:** Matching Pursuit; **NA:** Not Available; **OPs:** Oscillatory Potentials; **PCA:** Principal Component Analysis; **PERG:** Pattern Electroretinogram; **RGCs:** Retinal Ganglion Cells; **PhNR:** Photopic Negative Response; **PSD:** Power Spectral Density; **RP:** Retinitis Pigmentosa;**SD:** Standard Deviation; **STFT:** Short-Time Fourier Transform; **VEP:** Visual Evoked Potentials; **WA:** Wavelet analysis.

ACKNOWLEDGMENT

The authors thank Dr. Jila Hosseinkhani and Ms. Ankita Dey for their efforts in editing the manuscript at various stages.

REFERENCES

[1] S. M. Saszik, J. G. Robson, and L. J. Frishman, "The scotopic threshold response of the dark-adapted electroretinogram of the mouse," *J. Physiol.*, vol. 543, no. 3, pp. 899–916, Sep. 2002.

[2] J. Wu, A. D. Marmorstein, P. Kofuji, and N. S. Peachey, "Contribution of Kir4.1 to the mouse electroretinogram," *Mol. Vis.*, vol. 10, pp. 650–654, Sep. 2004.

[3] J. G. Robson and L. J. Frishman, "The rod-driven a-wave of the dark-adapted mammalian electroretinogram," *Prog. Retinal Eye Res.*, vol. 39, pp. 1–22, Mar. 2014.
[4] R. A. Stockton and M. M. Slaughter, "B-wave of the electroretinogram. A reflection of ON bipolar cell activity," *J. Gen. Physiol.*, vol. 93, no. 1, pp. 101–122, Jan. 1989.
[5] M. M. Azarmina, "Full-field versus multifocal electroretinography," *J. Ophthalmic Vis. Res.*, vol. 8, no. 3, pp. 191–192, 2013.
[6] D. C. Hood, M. Bach, M. Brigell, D. Keating, M. Kondo, J. S. Lyons, M. F. Marmor, D. L. McCulloch, and A. M. Palmowski-Wolfe, "ISCEV standard for clinical multifocal electroretinography (mfERG) (2011 edition)," *Documenta Ophthalmol.*, vol. 124, no. 1, pp. 1–13, 2012.
[7] D. J. Creel, "Multifocal electroretinograms," *J. Visualized Exp.*, vol. 58, p. 3176, Dec. 2011.
[8] M. Nebbioso, R. Grenga, and P. Karavitis, "Early detection of macular changes with multifocal ERG in patients on antimalarial drug therapy," *J. Ocular Pharmacol. Therapeutics*, vol. 25, no. 3, pp. 249–258, Jun. 2009.
[9] G. E. Holder, "Pattern electroretinography (PERG) and an integrated approach to visual pathway diagnosis," *Prog. Retinal Eye Res.*, vol. 20, pp. 531–561, Jul. 2001.
[10] R. Sharma, S. Joshi, K. D. Singh, and A. Kumar, "Visual evoked potentials: Normative values and gender differences," *J. Clin. Diagnostic Res.*, vol. 9, no. 7, pp. CC12–CC15, 2015.
[11] W. George and W. Bounds, "The electroretinogram: A review of the literature," *AMA Arch. Ophthalmol.*, vol. 49, no. 1, pp. 63–89, 1953.
[12] A. Balicka, A. Trbolová, and T. Vrbovská, "Electroretinography (a review)," *Folia Veterinaria*, vol. 60, no. 1, pp. 53–58, 2016.
[13] N. Pasmanter and S. M. Petersen-Jones, "A review of electroretinography waveforms and models and their application in the dog," *Vet. Ophthalmol.*, vol. 23, no. 3, pp. 418–435, May 2020.
[14] M. Drazek, M. Lew, S. Lew, and A. Pomianowski, "Electroretinography in dogs: A review," *Veterinarni Medicina*, vol. 59, no. 11, pp. 515–526, 2014.
[15] R. Tzekov and G. B. Arden, "The electroretinogram in diabetic retinopathy," *Surv. Ophthalmol.*, vol. 44, no. 1, pp. 53–60, Jul. 1999.
[16] K. G. P. Kumar, K. Karunakara, and G. S. Thyagaraju, "Automated identification of diabetic retinopathy—A survey," *Int. J. Recent Innov. Trends Comput. Commun.*, vol. 5, no. 6, pp. 514–520, 2017.
[17] U. Shankar and R. Gunasundari, "A review on electrophysiology based detection of diabetic retinopathy," *Procedia Comput. Sci.*, vol. 48, pp. 630–637, Jan. 2015.
[18] O. J. P. Charry and F. A. G. Osorio, "A systematic review of deep learning methods applied to ocular images," *Ciencia Ingeniería Neogranadina*, vol. 30, no. 1, pp. 9–26, Nov. 2019.
[19] A. E. Zhdanov, A. Y. Dolganov, V. N. Kazajkin, V. O. Ponomarev, A. V. Lizunov, V. I. Borisov, E. Lucian, X. Bao, and L. G. Dorosinskiy, "OculusGraphy: Literature review on electrophysiological research methods in ophthalmology and electroretinograms processing using wavelet transform," in *Proc. 8th IEEE Int. Conf. E-Health Bioeng. (EHB)*, Oct. 2020, pp. 1–6.
[20] W. A. Verdon, M. E. Schneck, and G. Haegerstrom-Portnoy, "A comparison of three techniques to estimate the human dark-adapted cone electroretinogram," *Vis. Res.*, vol. 43, pp. 2089–2099, Sep. 2003.
[21] J. Maguire, N. R. A. Parry, J. Kremers, I. J. Murray, and D. McKeefry, "The morphology of human rod ERGs obtained by silent substitution stimulation," *Documenta Ophthalmol.*, vol. 134, no. 1, pp. 11–24, Feb. 2017.
[22] L. J. Wilsey and B. Fortune, "Electroretinography in glaucoma diagnosis," *Current Opinion Ophthalmol.*, vol. 27, no. 2, pp. 118–124, Mar. 2016.
[23] N. V. Rangaswamy, L. J. Frishman, and E. U. Dorotheo, "Photopic ERGs in patients with optic neuropathies: Comparison with primate ERGs after pharmacologic blockade of inner retina," *Investigative Ophthalmol. Vis. Sci.*, vol. 45, no. 10, pp. 3827–3837, 2004.
[24] J. Tang, T. Edwards, J. G. Crowston, and M. Sarossy, "The test–retest reliability of the photopic negative response (PhNR)," *Transl. Vis. Sci. Technol.*, vol. 3, no. 6, p. 1, Oct. 2014.
[25] R. Granit, "The components of the retinal action potential in mammals and their relation to the discharge in the optic nerve," *J. Physiol.*, vol. 77, no. 3, pp. 207–239, Feb. 1933.
[26] M. Gauthier, M. Gauvin, J.-M. Lina, and P. Lachapelle, "The effects of bandpass filtering on the oscillatory potentials of the electroretinogram," *Documenta Ophthalmol.*, vol. 138, no. 3, pp. 247–254, Jun. 2019.
[27] M. F. Marmor, G. B. Arden, S. E. Nilsson, and E. Zrenner, "Standard for clinical electroretinography," *Arch. Ophthalmol.*, vol. 107, no. 6, pp. 816–819, 1989.
[28] D. L. McCulloch, M. F. Marmor, M. G. Brigell, R. Hamilton, G. E. Holder, R. Tzekov, and M. Bach, "ISCEV standard for full-field clinical electroretinography (2015 update)," *Documenta Ophthalmol.*, vol. 130, no. 1, pp. 1–12, Feb. 2015.
[29] M. F. Marmor, A. B. Fulton, G. B. Holder, Y. Miyaki, M. Brigell, and M. Bach, "The standard for clinical electroretinography (2008 update)," *Documenta Ophthalmol.*, vol. 118, no. 1, pp. 69–77, 2008.
[30] M. Sustar, G. E. Holder, J. Kremers, C. S. Barnes, B. Lei, N. W. Khan, and A. G. Robson, "ISCEV extended protocol for the photopic on-off ERG," *Documenta Ophthalmol.*, vol. 136, no. 3, pp. 199–206, Jun. 2018.
[31] H. H. Karimi, E. Jafarzadehpur, B. Blouri, H. Hashemi, A. Z. Sadeghi, and A. Mirzajani, "Frequency-domain electroretinography in retinitis pigmentosa versus normal eyes," *J. Ophthalmic Vis. Res.*, vol. 7, no. 1, pp. 34–38, 2012.
[32] W. Van Drongelen, *Signal Processing for Neuroscientists: An Introduction to the Analysis of Physiological Signals*. Amsterdam, The Netherlands: Elsevier. 2007.
[33] A. S. Al-Fahoum and A. A. Al-Fraihat, "Methods of EEG signal features extraction using linear analysis in frequency and time-frequency domains," *ISRN Neurosci.*, vol. 2014, Feb. 2014, Art. no. 730218.
[34] P. D. Welch, "The use of fast Fourier transform for the estimation of power spectra: A method based on time averaging over short, modified periodograms," *IEEE Trans. Audio Electroacoust.*, vol. AU-15, no. 2, pp. 70–73, Jun. 1967.
[35] P. P. Vaidyanathan, *The Theory of Linear Prediction*. San Rafael, CA, USA.: Morgan & Claypool, 2007.
[36] H. Baali, A. Khorshidtalab, M. Mesbah, and M. J. E. Salami, "A transform-based feature extraction approach for motor imagery tasks classification," *IEEE J. Transl. Eng. Health Med.*, vol. 3, 2015, Art. no. 2100108.
[37] C. W. Bresli and J. A. Parker, "Frequency spectrum analysis of the dark-adapted electroretinogram," *Can. J. Ophthalmol.*, vol. 7, no. 2, pp. 189–198, 1972.
[38] M. Gur and I. Gath, "Time and frequency analysis of simultaneously recorded corneal and non-corneal electroretinogram," *J. Biomed. Eng.*, vol. 1, no. 3, pp. 172–174, Jul. 1979.
[39] M. Gur and Y. Y. Zeevi, "Frequency-domain analysis of the human electroretinogram," *J. Opt. Soc. Amer.*, vol. 70, no. 1, pp. 53–59, 1980.
[40] K. Van Der Torren, G. Groeneweg, and G. Van Lith, "Measuring oscillatory potentials: Fourier analysis," *Documenta Ophthalmol.*, vol. 69, no. 2, pp. 153–159, Jun. 1988.
[41] X.-X. Li and N. Yuan, "Measurement of the oscillatory potentials of the electroretinogram in the domains of frequency and time," *Documenta Ophthalmol.*, vol. 76, no. 1, pp. 65–71, Nov. 1990.
[42] P. A. Sieving, E. B. Arnold, J. Jamison, A. Liepa, and C. Coats, "Submicrovolt flicker electroretinogram: Cycle-by-cycle recording of multiple harmonics with statistical estimation of measurement uncertainty," *Investigative Ophthalmol. Vis. Sci.*, vol. 39, no. 8, pp. 1462–1469, 1998.
[43] Z. H. Chen, C. W. Zheng, and B. Lei, "The extraction and analysis of a- and b-wave from electroretinogram in humans," *Chin. J. Ophthalmol.*, vol. 49, no. 12, pp. 1064–1068, 2013.
[44] A. Wood, T. Margrain, and A. M. Binns, "Detection of early age-related macular degeneration using novel functional parameters of the focal cone electroretinogram," *PLoS ONE*, vol. 9, no. 5, May 2014, Art. no. e96742.
[45] J. J. McAnany and P. R. Nolan, "Changes in the harmonic components of the flicker electroretinogram during light adaptation," *Documenta Ophthalmol.*, vol. 129, no. 1, pp. 1–8, Aug. 2014.
[46] J. Gotzmann, I. Dimopoulos, and Y. Sauve, "Contribution of oscillatory potentials to the on- and off-photopic electroretinogram (ERG) in humans," *Investigative Ophthalmol. Vis. Sci.*, vol. 55, p. 3510, Apr. 2014.
[47] C. Pahl, N. B. Mohammad, and E. Supriyanto, "Analysis on the electroretinography response for flickering and current stimulations," in *Proc. 38th Int. Conf. Telecommun. Signal Process. (TSP)*, Jul. 2015, pp. 482–485.
[48] M. V. Zueva, I. V. Tsapenko, O. S. Kolosov, D. V. Vershinin, V. A. Korolenkova, and A. D. Pronin, "Assessment of the amplitude-frequency characteristics of the retina with its stimulation by flicker and chess pattern-reversed incentives and their use to obtain new formalized signs of retinal pathologies," *Biomed. J. Sci. Tech. Res.*, vol. 19, no. 5, pp. 14575–14583, Jul. 2019.

[49] R. E. Poppele and L. Maffei, "Frequency analysis of the electroretinogram," *J. Neurophysiol.*, vol. 30, no. 5, pp. 982–992, Sep. 1967.
[50] M. Bach and T. Meigen, "Do's and don'ts in Fourier analysis of steady-state potentials," *Documenta Ophthalmol.*, vol. 99, no. 1, pp. 69–82, Sep. 1999.
[51] B. V. Bui, J. A. Armitage, and A. J. Vingrys, "Extraction and modelling of oscillatory potentials," *Documenta Ophthalmol.*, vol. 104, no. 1, pp. 37–55, 2002.
[52] H. A. Hancock and T. W. Kraft, "Oscillatory potential analysis and ERGs of normal and diabetic rats," *Investigative Ophthalmol. Vis. Sci.*, vol. 45, no. 3, pp. 1002–1008, 2004.
[53] J. Racine, S. Joly, M. Rufiange, S. Rosolen, C. Casanova, and P. Lachapelle, "The photopic ERG of the albino guinea pig (Cavia porcellus): A model of the human photopic ERG," *Documenta Ophthalmol.*, vol. 110, no. 1, pp. 67–77, Jan. 2005.
[54] N. V. Rangaswamy, W. Zhou, R. S. Harwerth, and L. J. Frishman, "Effect of experimental glaucoma in primates on oscillatory potentials of the slow-sequence mfERG," *Investigative Ophthalmol. Vis. Sci.*, vol. 47, no. 2, pp. 753–767, 2006.
[55] J. D. Akula, J. A. Mocko, A. Moskowitz, R. M. Hansen, and A. B. Fulton, "The oscillatory potentials of the dark-adapted electroretinogram in retinopathy of prematurity," *Investigative Ophthalmol. Vis. Sci.*, vol. 48, no. 12, pp. 5788–5797, 2007.
[56] J. M. Dai, Y. D. Chen, S. Y. Li, Z. Q. Yin, and C. H. Weng, "Frequency spectrum analysis of dark-adapted oscillatory potentials in normal rats," *J. Exp. Ophthalmol.*, vol. 30, no. 10, pp. 919–921, 2012.
[57] F. A. D. F. Rocha, B. D. Gomes, L. C. D. L. Silveira, S. L. Martins, R. G. Aguiar, J. M. de Souza, and D. F. Ventura, "Spectral sensitivity measured with electroretinogram using a constant response method," *PLoS ONE*, vol. 11, no. 1, Jan. 2016, Art. no. e0147318.
[58] Q. Quintana, M. L. Benedetto, M. M. Maldonado, A. C. V. E. de Payer, and M. A. Contin, "Electroretinography: A biopotential to assess the function/dysfunction of the retina," *J. Phys., Conf. Ser.*, vol. 705, Apr. 2016, Art. no. 012053.
[59] J. Dai, J. He, G. Wang, M. Wang, S. Li, and Z. Q. Yin, "Contribution of GABAa, GABAc and glycine receptors to rat dark-adapted oscillatory potentials in the time and frequency domain," *Oncotarget*, vol. 8, no. 44, pp. 77696–77709, Sep. 2017.
[60] B. Li, S. Grafe, A. Munchow, M. Lopez-Toledano, Z.-H. Pan, and W. Shen, "Sex-related differences in the progressive retinal degeneration of the rd10 mouse," *Exp. Eye Res.*, vol. 187, Oct. 2019, Art. no. 107773.
[61] A. F. Hussein, S. J. Hashim, A. F. A. Aziz, F. Z. Rokhani, and W. A. W. Adnan, "Performance evaluation of time-frequency distributions for ECG signal analysis," *J. Med. Syst.*, vol. 42, no. 1, p. 15, Jan. 2018.
[62] S. Nisar, O. U. Khan, and M. Tariq, "An efficient adaptive window size selection method for improving spectrogram visualization," *Comput. Intell. Neurosci.*, vol. 2016, Aug. 2016, Art. no. 6172453.
[63] S. Yu, X. You, W. Ou, X. Jiang, K. Zhao, Z. Zhu, Y. Mou, and X. Zhao, "STFT-like time frequency representations of nonstationary signal with arbitrary sampling schemes," *Neurocomputing*, vol. 204, pp. 211–221, Sep. 2016.
[64] M. Biswal and S. K. Mishra, "Comparison of time-frequency methods for analyzing stimulus frequency otoacoustic emissions," *J. Acoust. Soc. Amer.*, vol. 143, no. 2, pp. 626–639, Feb. 2018.
[65] D. Komorowski and S. Pietraszek, "The use of continuous wavelet transform based on the fast Fourier transform in the analysis of multi-channel electrogastrography recordings," *J. Med. Syst.*, vol. 40, no. 1, Jan. 2016, Art. no. 10.
[66] G. Liu, Y. Zhang, Z. Hu, X. Du, W. Wu, C. Xu, X. Wang, W. Wu, and S. Li, "Complexity analysis of electroencephalogram dynamics in patients with Parkinson's disease," *Parkinson's Disease*, vol. 2017, Feb. 2017, Art. no. 8701061.
[67] H. Witte and M. Wacker, "Time-frequency techniques in biomedical signal analysis: A tutorial review of similarities and differences," *Methods Inf. Med.*, vol. 52, no. 4, pp. 279–296, 2013.
[68] C. Baumgartner, K. Blinowska, A. Cichocki, H. Dickhaus, P. Durka, and P. McClintock, "Discussion of 'time-frequency techniques in biomedical signal analysis: A tutorial review of similarities and differences,'" *Methods Inf. Med.*, vol. 52, no. 4, pp. 297–307, 2013.
[69] J. Bardoňová, J. I. Provazník, and M. Nováková, "Matching pursuit decomposition for detection of frequency changes in experimental data—Application to heart signal recording analysis," *Scripta Medica*, vol. 79, nos. 5–6, pp. 279–288, 2006.
[70] A. Goshvarpour, A. Abbasi, and A. Goshvarpour, "An accurate emotion recognition system using ECG and GSR signals and matching pursuit method," *Biomed. J.*, vol. 40, no. 6, pp. 355–368, 2017.
[71] H.-X. Zhang, C.-F. Chen, Y.-L. Wu, and P.-H. Li, "Decomposition and compression for ECG and EEG signals with sequence index coding method based on matching pursuit," *J. China Univ. Posts Telecommun.*, vol. 19, no. 2, pp. 92–95, Apr. 2012.
[72] P. J. Durka, U. Malinowska, M. Zieleniewska, C. O'Reilly, P. T. Różański, and J. Żygierewicz, "Spindles in svarog: Framework and software for parametrization of EEG transients," *Frontiers Hum. Neurosci.*, vol. 9, p. 258, May 2015.
[73] S. Varadharajan, V. Lakshminarayanan, and K. Fitzgerald, "Wavelet analysis of ERG of patients with Duchenne muscular dystrophy," *Vis. Sci. Appl.*, pp. 65–68, 2000.
[74] S. G. Mallat, "A theory of multiresolution signal decomposition: The wavelet representation," *IEEE Trans. Pattern Anal. Mach. Intell.*, vol. 11, no. 7, pp. 674–693, Jul. 1989.
[75] T. Rogala and A. Brykalski, "Wavelet feature space in computer-aided electroretinogram evaluation," *Pattern Anal. Appl.*, vol. 8, no. 3, pp. 238–246, Dec. 2005.
[76] K. Penkala, "Analysis of bioelectrical signals of the human retina (PERG) and visual cortex (PVEP) evoked by pattern stimuli," *Bull. Polish Acad. Sci., Tech. Sci.*, vol. 53, no. 3, pp. 223–229, 2005.
[77] W. Zhou, N. Rangaswamy, P. Ktonas, and L. J. Frishman, "Oscillatory potentials of the slow-sequence multifocal ERG in primates extracted using the matching pursuit method," *Vis. Res.*, vol. 47, no. 15, pp. 2021–2036, Jul. 2007.
[78] S. Varadharajan, K. Fitzgerald, and V. Lakshminarayanan, "A novel method for separating the components of the clinical electroretinogram," *J. Mod. Opt.*, vol. 54, no. 9, pp. 1263–1280, Jun. 2007.
[79] K. Penkala, M. Jaskuła, and W. Lubiński, "Improvement of the PERG parameters measurement accuracy in the continuous wavelet transform coefficients domain," *Annales Academiae Medicae Stetinensis*, vol. 53, no. 1, pp. 58–60, 2007.
[80] R. Barraco, L. Bellomonte, and M. Brai, "Time-frequency behavior of the a-wave of the human electroretinogram," in *Proc. 11th Medit. Conf. Med. Biomed. Eng. Comput.*, Berlin, Germany, 2007, pp. 919–922.
[81] R. Barraco, D. P. Adorno, and M. Brai, "Wavelet analysis of human photoreceptoral response," in *Proc. 3rd Int. Symp. Appl. Sci. Biomed. Commun. Technol. (ISABEL)*, Nov. 2010, pp. 1–4.
[82] J. M. M. Jimenez, R. B. Velasco, L. B. Vazquez, J. M. R. Ascariz, and P. De la Villa Polo, "Multifocal electroretinography, glaucoma diagnosis by means of the wavelet transform," in *Proc. Can. Conf. Electr. Comput. Eng. (CCCEC)*, May 2008, pp. 867–870.
[83] J. M. Miguel-Jiménez, L. Boquete, S. Ortega, J. M. Rodríguez-Ascariz, and R. Blanco, "Glaucoma detection by wavelet-based analysis of the global flash multifocal electroretinogram," *Med. Eng. Phys.*, vol. 32, no. 6, pp. 617–622, Jul. 2010.
[84] J. M. Miguel-Jiménez, S. Ortega, L. Boquete, J. M. Rodríguez-Ascariz, and R. Blanco, "Multifocal ERG wavelet packet decomposition applied to glaucoma diagnosis," *Biomed. Eng. OnLine*, vol. 10, no. 1, p. 37, 2011.
[85] R. Barraco, D. P. Adorno, and M. Brai, "An approach based on wavelet analysis for feature extraction in the a-wave of the electroretinogram," *Comput. Methods Programs Biomed.*, vol. 104, no. 3, pp. 316–324, Dec. 2011.
[86] R. Barraco, D. P. Adorno, and M. Brai, "ERG signal analysis using wavelet transform," *Theory Biosci.*, vol. 130, no. 3, pp. 155–163, Sep. 2011.
[87] R. Barraco, D. P. Adorno, M. Brai, and L. Tranchina, "A comparison among different techniques for human ERG signals processing and classification," *Phys. Med.*, vol. 30, no. 1, pp. 86–95, Feb. 2014.
[88] I. S. Dimopoulos, P. R. Freund, T. Redel, B. Dornstauder, G. Gilmour, and Y. Sauvé, "Changes in rod and cone-driven oscillatory potentials in the aging human retina," *Investigative Ophthalmol. Vis. Sci.*, vol. 55, no. 8, pp. 5058–5073, 2014.
[89] S. S. Nair and K. P. Joseph, "Wavelet based electroretinographic signal analysis for diagnosis," *Biomed. Signal Process. Control*, vol. 9, pp. 37–44, Jan. 2014.
[90] M. Gauvin, J.-M. Lina, and P. Lachapelle, "Advance in ERG analysis: From peak time and amplitude to frequency, power, and energy," *BioMed Res. Int.*, vol. 2014, Oct. 2014, Art. no. 246096.

[91] J. M. Miguel-Jiménez, R. Blanco, L. De-Santiago, A. Fernández, J. M. Rodríguez-Ascariz, R. Barea, J. L. Martín-Sánchez, C. Amo, E. Sánchez-Morla, and L. Boquete, "Continuous-wavelet-transform analysis of the multifocal ERG waveform in glaucoma diagnosis," *Med. Biol. Eng. Comput.*, vol. 53, no. 9, pp. 771–780, Sep. 2015.
[92] H. Kundra, "Measurement of the photopic negative response of the electroretinogram by discrete wavelet analysis," M.S. thesis, Dept. Bioengineering, Univ. Illinois Chicago, Chicago, IL, USA, 2015.
[93] M. Gauvin, J. M. Little, J. M. Lina, and P. Lachapelle, "Functional decomposition of the human ERG based on the discrete wavelet transform," *J. Vis.*, vol. 15, no. 16, pp. 1–22, 2015.
[94] M. Gauvin, A. L. Dorfman, N. Trang, M. Gauthier, J. M. Little, J.-M. Lina, and P. Lachapelle, "Assessing the contribution of the oscillatory potentials to the genesis of the photopic ERG with the discrete wavelet transform," *BioMed Res. Int.*, vol. 2016, Dec. 2016, Art. no. 2790194.
[95] A. M. Alaql, "Analysis and processing of human electroretinogram," M.S. thesis, Dept. Elect. Eng., Univ. South Florida, Tampa, FL, USA, 2016.
[96] H. Kundra, J. C. Park, and J. J. McAnany, "Comparison of photopic negative response measurements in the time and time–frequency domains," *Documenta Ophthalmol.*, vol. 133, no. 2, pp. 91–98, Oct. 2016.
[97] M. Gauvin, "Time-frequency analysis of the human photopic electroretinogram: Method, normative data, and clinical applications," Ph.D. dissertation, Dept. Neuroscience, McGill Univ., Montreal, QC, Canada, 2017.
[98] L. M. Brandao, M. Monhart, A. Schötzau, A. A. Ledolter, and A. M. Palmowski-Wolfe, "Wavelet decomposition analysis in the two-flash multifocal ERG in early glaucoma: A comparison to ganglion cell analysis and visual field," *Documenta Ophthalmol.*, vol. 135, no. 1, pp. 29–42, Aug. 2017.
[99] H. Hassankarimi, S. M. R. Noori, E. Jafarzadehpour, S. Yazdani, and F. Radinmehr, "Analysis of pattern electroretinogram signals of early primary open-angle glaucoma in discrete wavelet transform coefficients domain," *Int. Ophthalmol.*, vol. 39, no. 10, pp. 2373–2383, Oct. 2019.
[100] S. Behbahani, A. Ramezani, M. K. Moridani, and H. Sabbaghi, "Time-frequency analysis of photopic negative response in CRVO patients," *Seminars Ophthalmol.*, vol. 35, no. 3, pp. 187–193, Apr. 2020.
[101] H. Ahmadieh, S. Behbahani, and S. Safi, "Continuous wavelet transform analysis of ERG in patients with diabetic retinopathy," *Documenta Ophthalmol.*, vol. 142, no. 3, pp. 305–314, Jun. 2021, doi: 10.1007/s10633-020-09805-9.
[102] J. D. Forte, B. V. Bui, and A. J. Vingrys, "Wavelet analysis reveals dynamics of rat oscillatory potentials," *J. Neurosci. Methods*, vol. 169, no. 1, pp. 191–200, Mar. 2008.
[103] J. Tomčala, "New fast ApEn and SampEn entropy algorithms implementation and their application to supercomputer power consumption," *Entropy*, vol. 22, no. 8, p. 863, Aug. 2020.
[104] A. Humeau-Heurtier, "Multiscale entropy approaches and their applications," *Entropy*, vol. 22, no. 6, p. 644, Jun. 2020.
[105] H. E. Hurst, "Long-term storage capacity of reservoirs," *Trans. Amer. Soc. Civil Eng.*, vol. 116, no. 1, pp. 770–799, Jan. 1951.
[106] T. V. Yakovleva, I. E. Kutepov, A. Y. Karas, N. M. Yakovlev, V. V. Dobriyan, I. V. Papkova, M. V. Zhigalov, O. A. Saltykova, A. V. Krysko, T. Y. Yaroshenko, N. P. Erofeev, and V. A. Krysko, "EEG analysis in structural focal epilepsy using the methods of nonlinear dynamics (Lyapunov exponents, Lempel–Ziv complexity, and multiscale entropy)," *Sci. World J.*, vol. 2020, Feb. 2020, Art. no. 8407872.
[107] S. Kesić and S. Z. Spasić, "Application of Higuchi's fractal dimension from basic to clinical neurophysiology: A review," *Comput. Methods Programs Biomed.*, vol. 133, pp. 55–70, Sep. 2016.
[108] B. Akbarian and A. Erfanian, "Automatic seizure detection based on nonlinear dynamical analysis of EEG signals and mutual information," *Basic Clin. Neurosci. J.*, vol. 9, no. 4, pp. 227–240, Aug. 2018.
[109] T. Heunis, C. Aldrich, J. M. Peters, S. S. Jeste, M. Sahin, C. Scheffer, and P. J. de Vries, "Recurrence quantification analysis of resting state EEG signals in autism spectrum disorder—A systematic methodological exploration of technical and demographic confounders in the search for biomarkers," *BMC Med.*, vol. 16, no. 1, Dec. 2018, Art. no. 101.
[110] N. Sefandarmaz, S. Behbahani, and A. Ramezani, "A novel method for electroretinogram assessment in patients with central retinal vein occlusion," *Documenta Ophthalmol.*, vol. 140, no. 3, pp. 257–271, Jun. 2020.
[111] D. W. Crevier and M. Meister, "Synchronous period-doubling in flicker vision of salamander and man," *J. Neurophysiol.*, vol. 79, no. 4, pp. 1869–1878, Apr. 1998.
[112] J. R. Etter, M. Walsh, and E. Chmeisser, "Focal electroretinogram (fERG) and chaos theory in the detection of glaucoma," *Investigative Ophthalmol. Vis. Sci.*, vol. 49, p. 2223, May 2008.
[113] S. S. Nair and K. P. Joseph, "Chaotic analysis of the electroretinographic signal for diagnosis," *BioMed Res. Int.*, vol. 2014, Jun. 2014, Art. no. 503920.
[114] M. Molaie, R. Falahian, S. Gharibzadeh, S. Jafari, and J. C. Sprott, "Artificial neural networks: Powerful tools for modeling chaotic behavior in the nervous system," *Frontiers Comput. Neurosci.*, vol. 8, p. 40, Apr. 2014.
[115] M. Sarossy, B. Aliahmad, and D. K. Kumar, "Timing of changes in the entropy of the electroretinogram with glaucoma," in *Proc. IEEE Life Sci. Conf. (LSC)*, Dec. 2017, pp. 95–98.
[116] D. Gabor, "Theory of communication. Part 1: The analysis of information," *J. Inst. Elect. Eng.-III, Radio Commun. Eng.*, vol. 93, no. 26, pp. 429–441, 1946.
[117] B. Toufik and N. Mokhtar, *The Wavelet Transform for Image Processing Applications*. Rijeka, Croatia: InTech, 2012.
[118] B. Falsini and V. Porciatti, "The temporal frequency response function of pattern ERG and VEP: Changes in optic neuritis," *Electroencephalogr. Clin. Neurophysiol./Evoked Potentials Sect.*, vol. 100, no. 5, pp. 428–435, Sep. 1996.
[119] J. B. Tary, R. H. Herrera, and M. van der Baan, "Analysis of time-varying signals using continuous wavelet and synchrosqueezed transforms," *Phil. Trans. Roy. Soc. A, Math., Phys. Eng. Sci.*, vol. 376, no. 2126, Aug. 2018, Art. no. 20170254.
[120] T. Zhao and W. Song, "An application of matching pursuit time-frequency decomposition method using multi-wavelet dictionaries," *Petroleum Sci.*, vol. 9, no. 3, pp. 310–316, Sep. 2012.
[121] S. Behbahani and M. K. Moridani, "Non-linear Poincaré analysis of respiratory efforts in sleep apnea," *Bratislava Med. J.*, vol. 116, no. 7, pp. 426–432, 2015.
[122] S. Behbahani, N. J. Dabanloo, A. M. Nasrabadi, C. A. Teixeira, and A. Dourado, "Pre-ictal heart rate variability assessment of epileptic seizures by means of linear and non-linear analyses," *Anadolu Kardiyoloji Dergisi/Anatolian J. Cardiol.*, vol. 13, no. 8, pp. 797–803, Oct. 2013.

SOROOR BEHBAHANI was born in 1983. She received the B.S., M.S., and Ph.D. degrees in biomedical engineering from Islamic Azad University, Science and Research Branch, Tehran, Iran.

Since 2013, she has been an Assistant Professor with the Electrical Engineering Department, Islamic Azad University, Garmsar Branch, Garmsar, Iran. She is currently an Assistant Professor with the Biomedical Engineering Department, Islamic Azad University, South Tehran Branch, Tehran. She is the author and a translator of two books and more than 50 articles. She is the holder of four patents. Her research interests include biomedical signal processing, machine learning, artificial intelligence, neuroscience, and chaos.

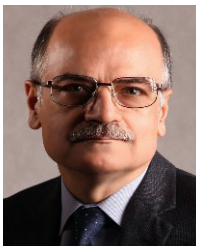

HAMID AHMADIEH was born in 1953.

He is currently an Ophthalmologist with a subspecialty in the medical and surgical retina. He is a Professor of ophthalmology at the Labbafinejad Medical Center, Shahid Beheshti University of Medical Sciences, Tehran, Iran. He is the Deputy Director of research at the Research Institute for Ophthalmology and Vision Science. His main research interests include retina and retinal cell biology. His awards are Razi Research Festival Award, in 2003 and 2018, the Achievement Award, the American Academy of Ophthalmology, in 2006, the Honor Award, the American Society of Retina Specialists, in 2010, the Senior Achievement Award, and the American Academy of Ophthalmology, in 2017.

SREERAMAN RAJAN (Senior Member, IEEE) received the B.E. degree in electronics and communications from Bharathiyar University, Coimbatore, India, in 1987, the M.Sc. degree in electrical engineering from Tulane University, New Orleans, LA, USA, in 1992, and the Ph.D. degree in electrical engineering from the University of New Brunswick, Fredericton, NB, Canada, in 2004.

From 1986 to 1990, he was a Scientific Officer with the Reactor Control Division, Bhabha Atomic Research Center (BARC), Bombay, India, after undergoing intense training in nuclear science and engineering from its training school. At BARC, he developed systems for control, safety, nuclear research, and power reactors regulation. From 1997 to 1998, he researched under a grant from Siemens Corporate Research, Princeton, NJ, USA. From 1999 to 2000, he was with JDS Uniphase, Ottawa, ON, Canada, worked on optical components and the development of signal processing algorithms for advanced fiber-optic modules. From 2000 to 2003, he was with Ceyba Corporation, Ottawa, Canada, where he developed channel monitoring, dynamic equalization, and optical power control solutions for advanced ultra-long-haul and long haul fiber optic communication systems. In 2004, he was with Biopeak Corporation, where he developed signal processing algorithms for non-invasive medical devices. From December 2004 to June 2015, he was a Defense Scientist with the Defence Research and Development Canada, Ottawa. He was an Adjunct Professor at the School of Electrical Engineering and Computer Science, University of Ottawa, Ottawa, from July 2010 to June 2018. He joined Carleton University as a Tier 2 Canada Research Chair (Advanced Sensors Systems and Signal Processing) of the Department of Systems and Computer Engineering, in July 2015, where he is currently a Full Professor. He has been an Adjunct Professor with the Department of Electrical and Computer Engineering, Royal Military College, Kingston, ON, Canada, since July 2015. He is the Director at Ottawa-Carleton Institute for Biomedical Engineering (OCIBME). He is the holder of two patents and two disclosures of the invention. He is the author of 175 journal articles and conference papers. His research interests include signal and image processing, biomedical signal processing, pattern classification, and applied machine learning. He has served as a Board Member for IEEE Canada, from 2010 to 2018. He was awarded the IEEE MGA Achievement Award, in 2012. He was recognized for his IEEE contributions with Queen Elizabeth II Diamond Jubilee Medal, in 2012. IEEE Canada recognized his outstanding service through 2016 W.S. Read Outstanding Service Award. He has been involved in organizing several successful IEEE conferences and has been a reviewer for several IEEE journals and conferences. He is the Chair of the IEEE Ottawa EMBS and AESS Chapters.